

# On-Site Scientific Presence at the Materials Research Collaborative Access Team

Carlo U. Segre, Illinois Institute of Technology, PI  
Bruce A. Bunker, University of Notre Dame, co-PI  
Randolph S. Duran, University of Florida, co-PI  
Pulak Dutta, Northwestern University, co-PI  
Jeff Terry, Illinois Institute of Technology, co-PI  
Mark Davidson, University of Florida, co-PI

January 10, 2003

## Abstract

The MR-CAT collaboration has been extremely productive over the past 3 years as a result of an on-site scientific presence which addresses the principal roadblocks to the effective use of a third generation x-ray source: the lack of familiarity with the operation of a synchrotron beamline by non-resident users; and the demands imposed by short beamtime allocations and rapid data collection on users who may have to reconfigure their experiments quickly in order to achieve their experimental goals. The MR-CAT on-site scientific staffing model has ensured that beam time used by CAT members and General Users is used effectively and results in scientific publications and student training. MR-CAT has therefore become a valuable research resource for x-ray spectroscopy, diffraction, microfocusing and *in-situ* studies. This proposal describes a selected few ongoing research projects which benefit directly from the presence of the MR-CAT scientific staff through scientific collaboration, development of new experimental techniques, or improvements to the current beamline which are only possible to make with a clear understanding of the scientific goals and scientific participation by on-site scientists. The research projects described herein span the topics of nanoscience, soft-hard matter interfaces and physical chemistry and demonstrate the scientific relevance and impact of the MR-CAT program. This research is funded at the home institutions but not at a level which would permit having an on-site presence at the beamline to ensure optimal use of the scarce beamtime resources. While the MR-CAT member institutions continue to make a financial commitment to the operation of this facility at the level of approximately 50% of the necessary operating funds, we seek DOE support to maintain the scientific productivity of this research resource and to significantly expand its capabilities on the operational insertion device line. A dedicated staff scientist is also sought to provide badly needed additional experimental capacity by assembling and commissioning the bending magnet first optical enclosure for routine spectroscopy.

# Contents

<b>1</b>	<b>Aims and Objectives</b>	<b>3</b>
<b>2</b>	<b>MR-CAT Achievements</b>	<b>4</b>
2.1	Results from Previous Funding . . . . .	4
2.2	Technical Milestones . . . . .	5
2.2.1	Monochromator . . . . .	5
2.2.2	Microfocusing . . . . .	5
2.2.3	Detectors . . . . .	5
2.2.4	Beam Cleaner . . . . .	6
2.2.5	Quick-Scan Powder Diffraction . . . . .	6
2.3	Educational Achievements . . . . .	6
<b>3</b>	<b>Scientific Program</b>	<b>6</b>
3.1	Overview . . . . .	6
3.2	Materials Science at the Nanoscale . . . . .	6
3.2.1	Size dependent alloying of core-shell nanoparticles in aqueous solution . . . . .	7
3.2.2	Electronic structure and morphology of fuel cell catalysts . . . . .	7
3.2.3	Photocatalytic metal-semiconductor interfaces . . . . .	11
3.2.4	Cu impurities in CdS/CdTe photovoltaic devices . . . . .	12
3.3	Soft-Hard Matter Interfaces . . . . .	15
3.3.1	Studies of metal ion binding and mineral growth at Langmuir monolayers . . . . .	16
3.3.2	Metal adsorption to biological and mineral surfaces . . . . .	17
3.3.3	Actinide fate and remediation . . . . .	18
3.3.4	Ordering of normal liquids at liquid-solid interfaces . . . . .	19
3.3.5	Nanoscale iron phases in neurodegenerative diseases . . . . .	20
3.4	Physical Chemistry . . . . .	24
3.4.1	Manganese and Vanadium molecular clusters . . . . .	24
3.4.2	Technetium Radiopharmaceuticals . . . . .	26
3.4.3	GIDX-ray Diffraction Of Polymerizing Langmuir Monolayers . . . . .	29
<b>4</b>	<b>Institutional Description</b>	<b>31</b>
<b>5</b>	<b>Budget Justification</b>	<b>31</b>
5.1	Staff Salaries . . . . .	31
5.2	Operational Costs . . . . .	32
<b>6</b>	<b>Biographical Sketches</b>	<b>33</b>
<b>7</b>	<b>References</b>	<b>43</b>

# 1 Aims and Objectives

The Materials Research Collaborative Access Team (MRCAT) Sector at the Advanced Photon Source (APS) synchrotron has been in operations on the undulator beamline since January of 1999 with the mission of studying complex materials and environmental systems *in situ*. Since spring of 2000, we have received a significant fraction (about 40%) of our operating budget from the DOE Office of Science, Basic Energy Sciences with the rest coming from member institutions making contributions. The funding from DOE has almost exclusively been used for salaries of scientists who have collaborated with researchers from our member institutions and with General Users (formerly called Independent Investigators by the APS). We have learned that such an on-site scientific presence is essential for the optimal use of x-ray beam time at this kind of facility for two reasons: the lack of familiarity of most users with MR-CAT and the rapid pace of experiments dictated by the MR-CAT scientific program.

Like all of the beamlines at the APS and other synchrotron sources in the United States, MR-CAT has the dual mission of providing research facilities for the members of the Collaborative Access Team (see section 4) and for the General User community which receives 25% of the beam time through a peer-reviewed proposal system. Many research programs at the MR-CAT member institutions have the potential to take advantage of the experimental techniques available at MR-CAT, however, the learning curve for effective use of this specialized facility is steep and researchers (often students and postdocs) who come to the beamline only once every three months are at a great disadvantage in properly designing and conducting their experiments in a way which maximizes the scientific productivity of the available beam time (usually 72 hours at a time). The situation of the General User is perhaps even more difficult as these scientists often obtain beam time at different beamlines from experiment to experiment and will, therefore, have even less opportunity to familiarize themselves with MR-CAT. Furthermore, few of these users will gain sufficient familiarity with the MR-CAT facility to effectively develop new instrumentation and improve the scientific performance of the beamline for their specific experiments.

The scientific program of the MR-CAT member institutions (see section 3) dictates the experimental capabilities and the kinds of General User experiments which are awarded beam time. The MR-CAT beamline is designed for x-ray spectroscopy, diffraction and microfocussing, including *in-situ* experiments. The nature of all of these experiments is that our users rarely stay at one energy, keep a single sample in the beam or even use a single experimental technique for more than 72 hours at a time (our typical beamtime allocation is 9 shifts of 8 hours each). For spectroscopy experiments, a user may change to multiple samples and more than one absorption edge. For diffraction and *in-situ* experiments, users often change samples every few hours or must continually change environmental conditions on a single sample. The high brilliance beam of an APS undulator has also led us to continually shorten the data acquisition time per sample in order to make the best use of the available beam time, leading to more frequent changes of sample or experiment during a typical 3-4 day run.

MR-CAT has addressed these two challenges by hiring a Ph.D. level scientific staff which is intimately familiar with the scientific goals of the collaboration as well as the capabilities of the beamline itself. It is this staff which is responsible for the scientific productivity of the MR-CAT facility by all of our users and for the continued development of our experimental capabilities. The role of the staff includes maintaining the operation of the beamline, improvement of current experimental systems, development of new techniques, assistance with experimental design and collaboration during and after the experiment. We seek, with this proposal, to increase the MR-CAT on-site staff, thereby, augmenting the scientific capabilities that all MR-CAT users can use to further the scientific goals of funded research programs at the participating institutions (MR-CAT members and General Users).

Over the past year, the MR-CAT insertion device beamline has become seriously oversubscribed. Our members have had to go to other beamlines to perform spectroscopy experiments because of insufficient time at MR-CAT and we have a limitation on the number of General users we can accommodate. In some cases the

spectroscopy experiments done at the MR-CAT insertion device could be adequately performed at an APS bending magnet. The MR-CAT member institutions have, therefore, been investing in equipment which could be utilized in the build out of the MR-CAT bending magnet. At this time we have nearly all of the equipment required for construction of a spectroscopy station in the First Optical Enclosure (FOE). This would provide badly needed additional capacity to our users.

The specific aims of this proposal are to:

- enable the best science to be accomplished at MRCAT by users who are not always resident at the facility;
- continue to drive improvements in efficiency and the development of new techniques;
- provide collaborations to General Users who would like to use the MR-CAT facilities; and
- install and commission spectroscopy capabilities in the bending magnet FOE.

The following sections will detail the technical and scientific achievements of MR-CAT to date and present short descriptions of research projects which require the on-site scientific presence in order to deliver the experimental results promised by the use of synchrotron radiation at a third-generation source.

## **2 MR-CAT Achievements**

### **2.1 Results from Previous Funding**

In the proposal for our current DOE funding, we presented six specific objectives:

1. enable the best science to be accomplished at MRCAT;
2. facilitate efficient set-up and operations of a variety of complex materials-related experiments;
3. open the beamlines' facilities to scientists and science projects from non-traditional backgrounds and disciplines respectively;
4. enable efficient 24 hour use of the beamline through interdisciplinary research teams and appropriate operations support;
5. develop selected operations modes, in support of the MRCAT institutions, DOE collaborators, and general users; and
6. achieve user operations status in both beamlines of the MRCAT sector.

We believe that, with the exception of item 6, we have met all of our objectives. MR-CAT scientists have published 42 papers as of the end of FY02, including articles in the most prestigious journals in their respective fields. MR-CAT has established a scheduling process which groups similar techniques in order to avoid changeovers between widely varying experiments. The changeovers from one technique to another have also been streamlined and generally require less than 8 hours of time which we try to spend during times when the beam is not available. We have made a concerted effort to recruit users new to synchrotron radiation both at our institutions and as General Users. The MR-CAT beamline has been scheduled for 24 hour operation for the past 3 years. The only down time is when there is a beamline system failure or when we are commissioning new equipment (although we attempt to perform commissioning experiments 24

hours a day whenever possible). Our resident scientists have assisted in developing specialized equipment needed by our users, collaborated with users as they come on site and with users who are unable to travel to the beamline (including General Users). The MR-CAT institutions have accumulated the funds necessary to instrument the First Optical Enclosure of the bending magnet line but a shortage of resident users has made it impossible to put the effort into final design and construction of this beamline to date.

All of these accomplishments have been made possible by our having a dedicated scientific staff resident at MR-CAT. Experience at many sectors of the APS has shown that the presence of resident scientific staff correlates directly with the scientific productivity of the beamline. Our scientific staff is small but has enabled us to be very productive as a collaboration.

## **2.2 Technical Milestones**

### **2.2.1 Monochromator**

We now have the capability of running our monochromator in pseudo fixed exit mode and of running spectroscopy quick scans reliably in times as low as 4 seconds using the encoder readouts for energy calibration. This is now our standard mode of operation and will permit us to work with samples that are severely damaged in the undulator beam or in situations where sample conditions change on a time scale of minutes. We have had a polished set of crystals in the monochromator for the past 2 years with no need to replace the cryogenic seals. This development is a result of long collaboration between interested users our software specialist and the resident scientists who have put a large amount of time in building interfaces and testing the operation of this mode of operation.

### **2.2.2 Microfocusing**

The development of microfocussing capabilities at MR-CAT has been led by one of our resident scientists over the past 3 years. We made an early decision to implement the microfocusing capability using Kirkpatrick-Baez mirrors in order to be able to carry out both fluorescence mapping and spectroscopy at moderate spot sizes. This project has been successfully completed and microfocussing is now a regularly scheduled mode of operation for the beamline. The design of the microfocussing system is such that it can be completely removed from the beamline and then reinserted and realigned within a matter of hours. Our current focal spot is about  $5\mu \times 5\mu$  but we plan to obtain a further reduction by purchasing a higher quality set of mirrors. Fluorescence mapping and spectroscopy experiments have become routine and there are plans to add further functionality to the system in the form of micro-diffraction.

### **2.2.3 Detectors**

We have successfully implemented data acquisition and control of our 13-element solid state detector in step scan mode. With further development of the control software we expect to be able to acquire data with this detector in continuous scan mode, in the same way as we perform routine EXAFS. The performance of the detector and electronics is excellent, having achieved overall count rates of nearly  $2 \times 10^6$  counts per second per channel, far outstripping the specified values of  $4 \times 10^5$ . We have been able to measure the fluorescence edge of no more than 10ng of Pu in a sample with significant background and this detector system is being used by General users as well A MR-CAT members. We have also continued development of the bent Laue analyzer for fluorescence detection (we are currently at the third revision of the design) and some of our users routinely use this analyzer for experiments where there is high background or closely spaced fluorescence lines.

## 2.2.4 Beam Cleaner

We have fabricated an initial design of a bent Laue crystal optic for use in removing harmonics and subharmonics from a high energy (>40keV) beam. We often need high energy beams (up to 80keV) for powder diffraction and pair distribution function experiments. These energies are obtained by using the (333) reflection of the Si monochromator crystal. The beam that comes into the hutch, therefore, contains not only the desired energy  $E$  but  $E/3$ ,  $2E/3$ ,  $5E/3$ ,  $7E/3$ ,  $3E$ , and so on. X-ray mirrors will not work above about 30keV and in any case a mirror cannot remove the undesirable, and intense sub-harmonics. By using a pair of bent Ge crystals diffracting from the (111) planes, it is possible to remove all the undesired energies except the  $3E$  (which is not very intense for  $E=80\text{keV}$ ). We have done initial testing of this device and measured a nearly 50% reflectivity of the desired energy at 80keV. More recently, a powder diffraction pattern of  $\text{LaB}_6$  has been obtained using 80keV radiation from this beam cleaner.

## 2.2.5 Quick-Scan Powder Diffraction

We have extended the continuous scan capability to two motors on the Huber 8-circle goniometer. One of these is the delta motor which scans the  $2\theta$  angle in a powder diffraction experiment. Coupled with the custom capillary spinner we have developed to rotate a filled capillary at high speeds (several hundred RPM), we have added routine powder diffraction experiments to our capabilities. The second goniometer motor which can be continuously scanned is the horizontal motion of the detector arm. This permits us to study the diffuse scattering from liquid surfaces in short times.

## 2.3 Educational Achievements

Student training has become a significant aspect of the MR-CAT activities. To date, we have had 37 students at the beamline and 11 of them have received their degrees. At the 2001 APS Users Meeting, the User Executive Committee listed 43 students who had received their Ph.D.s and had conducted significant portions of their research at APS beamlines. Of these 43, 6 had used MR-CAT. This disproportionately high fraction ( $\sim 14\%$ ) is indicative of the commitment that MR-CAT institutions have to student participation and training. In addition, we have also had 4 Undergraduate summer interns spend time at the MR-CAT beamline in 2001 and two more in 2002. The work done by Undergraduate students will result in at least 3 publications in 2003. We hope to continue to make these opportunities available in future years.

# 3 Scientific Program

## 3.1 Overview

The following brief scientific descriptions show the kind of innovative research that we intend to pursue at MR-CAT. We have grouped the projects into three categories: nanoscale science, soft-hard interfaces and physical chemistry. Since much of the science done at MR-CAT is interdisciplinary, there is much more overlap than this somewhat arbitrary categorization implies. The complexity of the experiments described serves to illustrate the need to have resident scientists at MR-CAT who will take responsibility for the successful development of experimental techniques and completion of the experiments.

## 3.2 Materials Science at the Nanoscale

The study of materials at nanometer-sized dimensions is one of the most exciting and well-publicized research areas in the physical sciences. The novel properties of nanoscale materials derive from the physical

dimensions of the materials and their structural and electronic consequences. X-ray absorption spectroscopy (XAS) is an ideal characterization method for such materials as it permits study of both the structural and electronic properties by probing the electronic states of the absorbing atom and the local structure surrounding it. In nanoscale materials there typically are subtle changes in the electronic states and local structure which are difficult to probe with other characterization techniques. The MR-CAT beamline operates at the ideal length scale and with an x-ray brilliance for this kind of research. Furthermore, because it has been specifically designed for XAS and *in-situ* experiments, the MR-CAT facility is uniquely suited to the study of nanoscale materials and there are a number of projects already taking advantage of it. With the following project descriptions, we attempt to give a flavor of the kinds of nanoscale research we plan to conduct and which will benefit from an on-site scientific staff at MR-CAT.

### 3.2.1 Size dependent alloying of core-shell nanoparticles in aqueous solution

The interface structure of the bimetallic core-shell nanoparticles is important for the optical and catalytic properties. In collaboration with the DOE-funded Notre Dame Radiation Laboratory, we have been using XAFS (in addition to other techniques) to study the properties of radiolytically-produced nanoparticles suspended in aqueous solution. Our initial studies have been of (initial) gold-core / silver-shell nanoparticles, investigating interdiffusion and other structural properties. From the systematic studies of the particle size dependence (various core size and shell thickness), we found a remarkable size-dependent alloy formation at room temperature.[1] Figure 1 shows the Au  $L_{III}$  edge XAFS oscillations,  $\chi(k)$ , and their Fourier transforms for 2.5 nm pure Au, and 2.5 nm Au core nanoparticles initially coated with 1.1, 3.8 and 6.5 atomic layers of Ag. Note the change of the oscillatory features above approximately  $k = 6\text{\AA}^{-1}$  with the increase of the Ag deposition.

This change in  $\chi(k)$  appears clearly in the Fourier transform as the change of intensity ratio of the doublet features highlighted by the arrows. The peak intensity at larger distance increases relative to that of the peak at smaller distance with increasing Ag deposition due to changes in interference between the Au and Ag oscillations. Note that both peaks come from the first neighbor (with a single distance) and they appear at a shorter distance from the actual bond lengths because of the backscattering phase. Figure 2 shows the fraction of Ag near neighbors around Au as a function of initial Au nanoparticle size. The nanoparticles with initial Au core diameter larger than 8.3nm retain the core-shell structures in equilibrium. On the other hand, for the particles with the initial core size smaller than 4.6nm, a significant mixing of the atoms was observed within several days. Even in the latter case, the mixing (alloying) is mainly limited to the region close to the initial interface. This results from the increase of the Ag near-neighbors around Au atoms, since Au and Ag have quite different backscattering phase shifts at higher  $k$ . These findings cannot be explained by a bulk diffusion process or surface melting, but rather lead us to a size-dependent solid state alloying mechanism. The molecular dynamics simulation shows a very small amount of vacancies at the interface (less than 1%) will accelerate the atomic diffusion and explain the observed fast diffusion.

This work will be continued and expanded, with studies of different metallic combinations such as Pd/Au and Pt/Au and as a function of temperature. While the initial studies were done in solution, in the next level of studies we will also investigate precipitates of  $\text{SiO}_2$ -capped and thiol-chemisorbed nanoparticles, enabling enable a much wider range of measurement and annealing temperatures. Although some of these studies will involve bulk XAFS, we will also be using grazing-incidence "evanescent wave" XAFS to study nanoparticles on surfaces to further investigate particle-substrate interactions.

### 3.2.2 Electronic structure and morphology of fuel cell catalysts

Polymer electrolyte fuel cells (PEFCs) are prime candidates for next generation power sources for portable power, automobile and residential applications. The PEFC fuel, be it gaseous or liquid, contains carbon

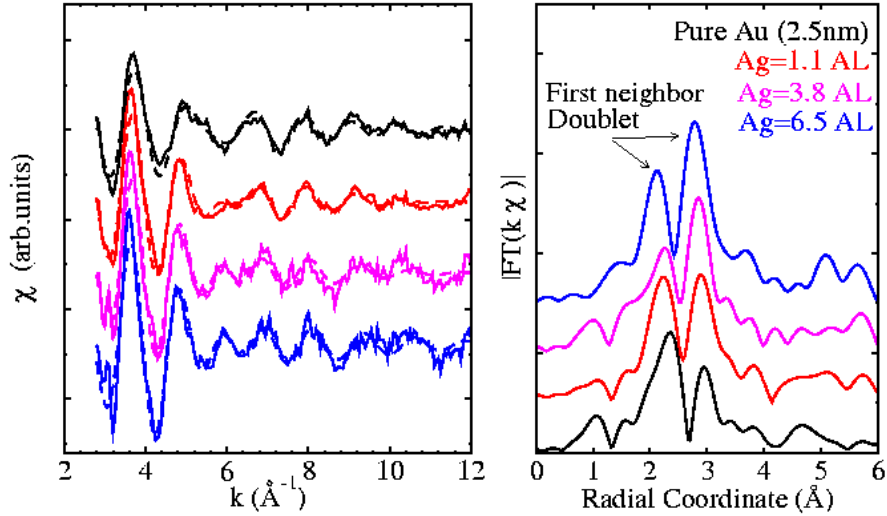


Figure 1: **(A)** Au  $L_{III}$  edge XAFS oscillations,  $\chi(k)$ , for 2.5 nm pure Au, and 2.5 nm Au core nanoparticles initially coated with 1.1, 3.8 and 6.5 atomic layers of Ag. Experimental spectra (dotted lines) are shifted along the y-axis for clarity. The fits for the Au/Ag first neighbors are also shown (solid lines). **(B)** Magnitude of the Fourier transform of  $\chi(k)$  for the samples shown in (A), where  $3^{-1}\text{\AA} < k < 11^{-1}\text{\AA}$  is transformed. The spectra are shifted vertically for clarity.

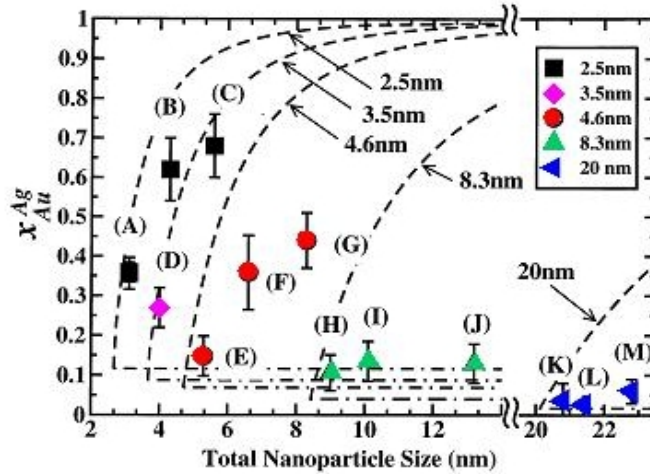


Figure 2: The fraction of Ag near neighbors around Au,  $x_{Ag}^{Ag}$ , as a function of total nanoparticle size for various initial Au-core sizes and with various Ag thickness. Different initial Au-core sizes are depicted as different symbols. Dashed curves indicate a random alloy for the corresponding initial core size. Dashed straight lines indicated phase segregated core-shell structures. These results are inconsistent with simple diffusion models of Au/Ag in the nanoparticles.

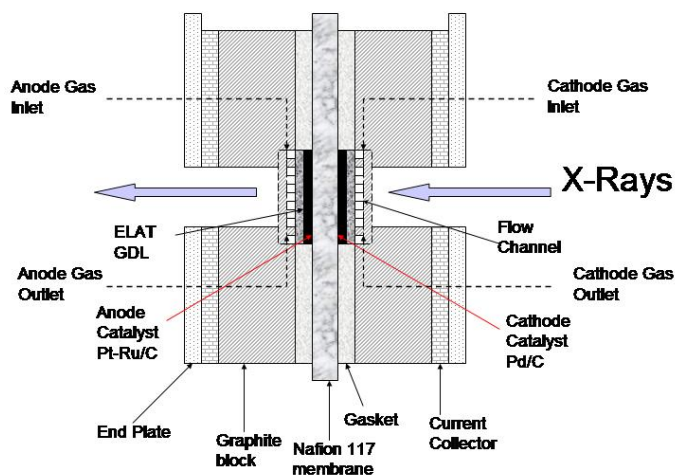


Figure 3: Schematic of modified fuel cell for in-situ XAS experiments.

monoxide which is adsorbed onto the catalyst surface blocking active sites for fuel oxidation. The best-known CO tolerant catalysts are Pt-Ru in particles of nanometer dimension.[2, 3] While there have been a number of studies of such particles by *ex-situ* EXAFS,[4, 5, 6, 7, 8] little is known about the morphology of supported Pt-Ru catalysts in the working fuel cell. A range of possibilities includes disordered bimetallic alloys to multiple phases (including alloys and oxides). For example, studies on high surface area Pt-Ru electrocatalysts have reported that the lattice parameters of high surface area mixed metal catalysts were larger than that observed in arc-melted alloys.[9] Equivalence of the lattice parameter of the nanostructured pure Pt catalyst with that of the arc-melted pure Pt confirms that there is no lattice contraction associated with catalyst particles in the size domain of fuel cell catalysts (i.e. 2 - 3 nm), thus the larger lattice parameters must result from phasing out of some of the smaller atoms of Ru from the alloy phase leaving a Pt rich alloy with a correspondingly higher lattice parameter.

Until recently, the only way to probe the structure of fuel cell catalysts has been through powder diffraction and *ex-situ* x-ray spectroscopy. Our work at MR-CAT, in collaboration with Eugene Smotkin of the University of Puerto Rico and Simon Bare of UOP, has shown that it is possible, at a third generation source, to obtain *in-situ* XAFS data on a working fuel cell.[10] This opens up a vast area of study which will lead to a detailed understanding of the mechanisms which affect catalyst performance.

Using a modification of a high performance single cell fuel cell,[11] (Figure 3) we obtained data at the Pt  $L_{III}$  and Ru K edges. The fuel cell was operated with pure  $H_2$  and reformat simulant at the anode. Pd/C was used at the cathode (instead of the usual Pt/C) in order to measure absorption only from the Pt at the anode. Because of this choice of cathode, the  $H_2$ -air cell performance is inferior to a standard cell but this does not affect the performance of the anode half-cell. Multiple transmission X-ray Absorption Near Edge Spectroscopy (XANES) scans of 2-5 minutes each were taken at identical fuel cell operating conditions and were signal averaged prior to normalization. Figure 4 shows the XANES data for the Pt  $L_{III}$  edge on a conditioned and unconditioned MEA and a Pt foil reference. The data show a characteristic Pt white line at 11564 eV and the spectral features at all conditions are essentially identical to that of metallic Pt. Thus under typical fuel cell operating conditions anode Pt (incorporated in an alloy phase) is fully reduced. Pt  $L_{III}$  edge XANES of a conditioned and unconditioned MEA at selected fuel cell operating conditions with reformat simulant is virtually identical, confirming that Pt is still metallic in the alloy irrespective of whether the anode gas is neat  $H_2$ , reformat simulant with either conditioned or fresh MEAs. Beyond the XANES region and into the X-ray Absorption Fine Structure (XAFS) region, which contains the local structure information, the spectra show significant deviation from that of Pt metal. This is due to the presence of the Ru in the

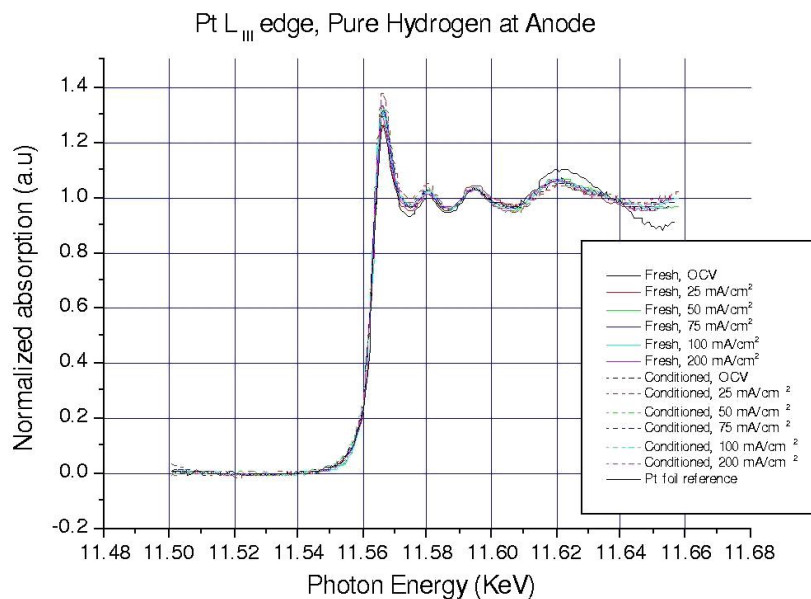


Figure 4: Pt  $L_{III}$ -edge XANES spectra for pure  $H_2$  at the anode of a Fresh MEA Conditioned MEA at various current densities. The white line intensity does not correlate with current density. We believe that the differences in the white line intensity reflect the reproducibility of the spectra recorded in-situ with the present experimental arrangement rather than differences in the electronic structure of the Pt.

catalyst and to the fact that the catalyst particles have dimensions of about 4nm. Close inspection of the white line region of the spectra reveal that the area under the curve for the MEAs under all conditions is greater than for the Pt foil. This small but systematic effect reflects the reduction in occupied Pt d-states when alloyed with Ru and is consistent with the results of McBreen and Mukerjee.[5] The implications of this on our understanding of the mechanisms for CO adsorption to the catalyst are profound. Initial calculations using Density Functional Theory indicate that this reduction of occupied d-states is consistent with the reported decrease in stretching frequencies of adsorbed CO,[12] contrary to the previously accepted Blyholder model.[13]

The Ru XANES with neat  $H_2$  (the reformate simulant data are identical) is shown in Figure 5 with Ru metal and  $RuO_2$  included as reference. Again, the data show that Ru is in the metallic state at all operating conditions. The fact that there are no changes in the XANES on a fresh and conditioned MEA at different current densities indicates that the Pt-Ru catalyst is easily reduced to its metallic state upon contact with  $H_2$ . It should also be noted that the electrode was polarized anodically to ensure  $H_2$  or reformate oxidation. The above results are consistent with that of O'Grady et. al. who reported metallic phases on Pt  $L_{III}$  and Ru K edges on a supported Pt-Ru catalyst.[4] In an *ex-situ* study, both a fresh MEA (as prepared) and a conditioned MEA re-exposed to air show the presence of some oxide in the Ru K edge, however they are not identical, indicating that the conditioning process may alter the morphology in such a way as to limit the re-oxidation of the Ru.

The characteristics of the MR-CAT beamline are essential for the successful acquisition of this kind of *in-situ* data. The nafion membrane in a PEFC requires constant humidification and therefore, there is a continual formation of water droplets as the gas changes temperature while traversing the fuel cell flow field. The presence of these water droplets significantly changes the x-ray absorption of the fuel cell and leads to an unstable baseline in the XAFS spectra. With careful adjustment of the fuel cell and gas feed

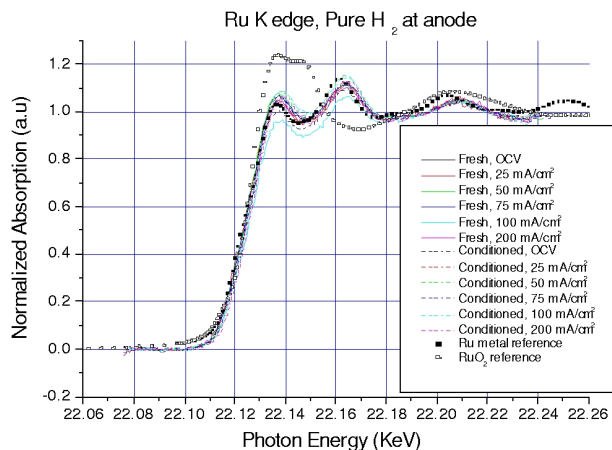


Figure 5: Ru K-edge XANES spectra for pure H<sub>2</sub> at the anode of a Fresh MEA and Conditioned MEA at various current densities superimposed on Pt foil and Pt<sub>80</sub>Ru<sub>20</sub> bulk alloy references.

temperatures, we have found that it is possible to reduce the frequency of droplet formation, however, data taken in conventional step scanning mode (the only mode possible at second generation synchrotron sources or at an APS bending magnet) will inevitably have at least one droplet in the 30 minutes it takes for the complete spectrum. The high brilliance of the APS undulator and the continuous scanning mode available at MR-CAT (less than 1 minute per spectrum), is therefore, the only way to obtain usable data on such a system. Even so, the use of transmission mode severely limits the quality of the XAFS data, particularly at the Ru edge where the absorption of even a dispersed 50-50 alloy of Pt-Ru is very small. As we continue this project, we will redesign the fuel cell to permit us to take data in fluorescence mode. This will improve the signal at the Ru edge and permit a detailed structural analysis of the Pt-Ru catalysts *in-situ*. We will use FEFF8 [21] to model the Pt-Ru particles and the adsorbed CO to better understand the role of Ru in improved catalyst performance. By analysis of both the XANES and XAFS data, we will begin to measure the morphology of the Pt-Ru nanoparticles during conditioning and extended MEA operation.

The studies described above have all been performed on commercially available catalysts. Our ultimate goal is to extend the studies to new catalytic materials which are been developed and tested by our collaborators using combinatorial techniques. Of particular interest are catalysts in the ternary Pt-Ru-Os system which have shown promise. A key parameter for high performance is the Pt-Pt bond length which in pure Pt is too large for efficient O-O bond breaking. The addition of Ru serves to reduce the Pt-Pt bond length and XAFS, being particularly sensitive to this quantity, is an ideal probe.

### 3.2.3 Photocatalytic metal-semiconductor interfaces

It has been observed that the deposition of noble metal on the surface of semiconductor nanoparticles greatly enhances the photocatalytic performance. This beneficial effect appears basically in two ways - 1) enhancement of charge rectification in a UV-irradiated semiconductor by forming a Schottky junction and 2) doping of metals modifies the energetics of the semiconductor in a way that the bandgap of the semiconductor reduces from UV- regime to visible. These effects have tremendous applications in solar-cells and other environmental problems such as hydrogen generation from hydrolysis. However, the catalytic performance degrades over time (as fast as 15 minutes) and questions their long-term performance.

We have investigated such a nano-composite system under varying periods of UV-irradiation and observed a remarkable change in the interface following irradiation. The samples included titania as the nano-structured

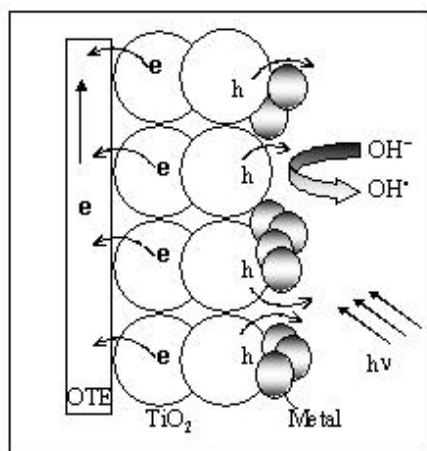


Figure 6: Formation of Au ions from oxidation by holes and hydroxyl radicals at the TiO<sub>2</sub>/Au interface and its possible role as recombination center. Some of the electrons are attracted towards Au ions instead of flowing to the electrode, thus reducing the photocurrent.

semiconductor film (average particle size of 20 nm) with noble metals like Au, Pt or Ir (particle size of 8 nm) deposited on them electrophoretically. After UV-irradiation, the system was treated with NaCN to leach off excess nanoparticle, leaving only the remnant metal at the interface. The XANES of the samples interestingly indicates a positive oxidation state of these noble metals which renders them as recombination centers for photo-excited electrons (see Figure 6). The oxidation can be attributed to the holes or surrounding hydroxyl radicals in solution. Thus in a photo-excited nano-composite, oxidation and reduction processes compete in parallel to determine the ultimate fate of the system.

The EXAFS results indicate an intercalation of the noble atoms into the semiconductor. The near-neighbor species around the atoms also change depending on the noble metal in question. For example, Au forms a cluster within the interface (see Figure 7) while Pt fails to show such clustering effect. Rather, a correlation of Pt with O is observed over a longer distance while this correlation is not observed in the case of Au. Ir behaves yet differently in that it does not exhibit clustering effect as well as it does not show any Ti correlation over a shorter distance, unlike the other two metals. The difference in near-neighbor species in different systems affects the charge-distribution and charge-trapping and alters their energetics. Thus structural findings may explain the different photocatalytic performances of these various nano-composite systems.

Although we have initial results submitted for publication, these experiments are in the initial stages. More careful systematic studies as function of metal species, radiation conditions, nanoparticle morphology, etc. are still planned. Depending on the particular sample, these experiments involve traditional fluorescence XAFS, x-ray reflectivity, and/or grazing-incidence evanescent-wave XAFS.

### 3.2.4 Cu impurities in CdS/CdTe photovoltaic devices

Photovoltaic devices can be used to generate electricity from a clean, renewable energy source, the sun. However, current photovoltaic devices have low conversion efficiency due to extrinsic defects such as Cu and Na impurities. In CdTe, Cu is often used as part of a back contact preparation but Cu easily migrates to the CdS/CdTe junction region and into the CdS during processing and perhaps during cell operation.[72] Furthermore, its chemical state and electrical activity can be changed by moderate light soak and recovered again by subsequent heat treatments.[73] In our preliminary work, we have used ion implantation with photoluminescence (PL), electroluminescence, x-ray spectroscopies (Fluorescence and Absorption) to improve

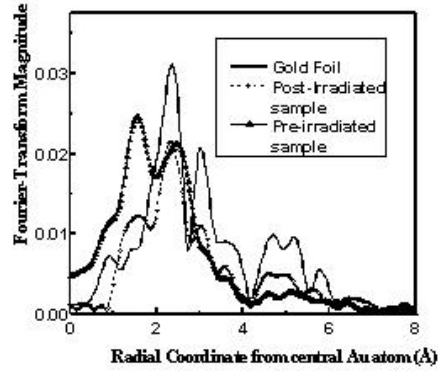


Figure 7: The Fourier transform of  $\chi(k)$  for  $\text{TiO}_2/\text{Au}$  samples with and without UV illumination shown with Au foil. The  $\text{TiO}_2/\text{Au}$  samples show a low distance peak from oxygen neighbors which is absent in Au foil; At higher distances the sample with UV is similar to Au foil indicating a clustering of Au atoms by UV light while such cluster feature is absent in the sample without UV.

our understanding of Cu impurities in CdTe grown on either float glass or quartz substrates. These measurements have been a collaborative effort with the University of Toledo Physics Department (Al Compaan and Xiangxin Liu).

Our PL studies were done with the 488 nm line of an Ar ion laser to provide excitation depth nearly matching the projected range of implantation. The lowest density implant,  $1 \times 10^{16} \text{ cm}^{-3}$ , shows additional PL bands even before annealing if a careful subtraction is done relative to the adjacent unimplanted region. To heal the damage due to high-energy ion implantation, these samples were annealed in flowing  $\text{N}_2$  successively at  $350^\circ$ ,  $375^\circ$ ,  $400^\circ$ . The PL signal, which reached its maximum after the third anneal at  $400^\circ\text{C}$ , is shown for the lowest Cu density sample in Figure 8.

The data from the Cu-implanted regions clearly show two peaks each of which appears to be blended. Peaks can be identified at 1.498eV and 1.476eV blended with additional peaks approximately 8meV higher in each case. The peak separation of about 21meV suggests a phonon replica; the power dependence suggests that these peaks arise from near pairs with a high recombination rate.

Synchrotron x-ray fluorescence was used to determine the amount of Cu impurities in the CdTe films and substrates (Quartz, BSG, SLG). Films of CdTe  $2\text{-}3\mu\text{m}$  thick were magnetron sputtered onto borosilicate glass slides. The Cu  $\text{K}_\alpha$  fluorescence at 8.05keV from these films was excited by the x-ray beam at 9.5keV, above the K-absorption edge of Cu at 8.98keV. These measurements showed a significant amount of Cu in the substrates.

As a first step in understanding the properties of Cu impurities, we have taken preliminary XAS data on CdTe films on a Quartz substrate with and without  $\text{CdCl}_2$  treatments, which are known to improve the performance of CdTe solar cells.[76, 77] Figure 9 shows the XAS transforms from both  $\text{CdCl}_2$  treated samples and untreated samples. The transforms are related to the radial distribution function of the material. They clearly show that the local structure around the Cu atoms was different between  $\text{CdCl}_2$  treated samples and untreated samples on a quartz substrate. This suggests that the local structure of the impurity in the substrate may be a large factor in the device properties.

We plan to extend this study by careful selection of substrates, *in-situ* annealing studies and controlled  $\text{CdCl}_2$  treatments. Specifically, we will perform the x-ray measurements while the University of Toledo will be responsible for synthesis and EL and PL measurements. We expect Cu impurities to be present in the substrates at concentrations of ppm or less. In order to make the XAS measurements at these low concentrations, it is necessary to utilize undulator radiation coupled with a Multielement Ge Detector. MR-

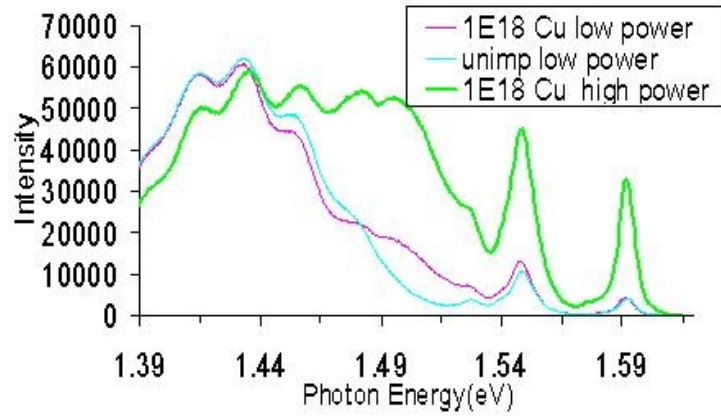


Figure 8: PL from Cu-implanted CdTe crystal samples after annealing, both unimplanted and implanted regions with low and high laser power @ 488nm.

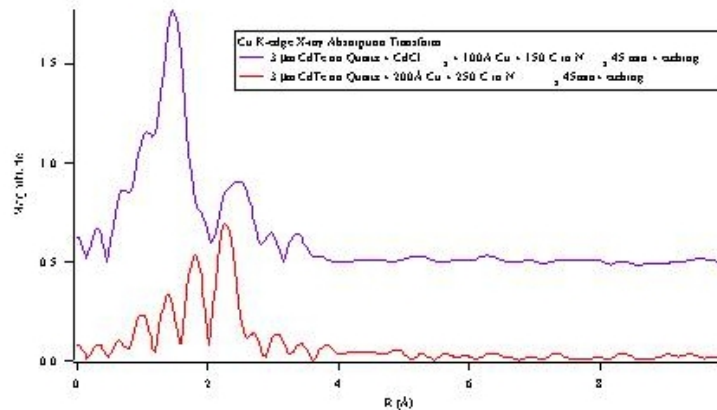


Figure 9: Transform of Cu K-Edge x-ray absorption from CdCl<sub>2</sub> treated and untreated samples on a Quartz substrate.

CAT is a perfect facility for these difficult measurements.

We will initially measure the Cu K-edge, x-ray absorption spectra from the bare substrates, Kapton, Borosilicate glass (BSG), soda-lime glass (SLG), and Quartz. BSG, SLG, and Quartz are all typical CdTe device substrates while Kapton has been added as a substrate due to its extremely low, sub-ppb, concentration of Cu in Kapton foil. Kapton can also withstand the growth and annealing temperatures of the CdTe photovoltaic devices. As Kapton is flexible and strong material, it may be a novel substrate for the development of new CdTe devices.

The *in-situ* measurements will be performed on substrates exposed to either CdCl<sub>2</sub> vapor or a saturated solution of CdCl<sub>2</sub> in methanol. Cu K-edge XAS measurement will be collected as a function of temperature as the substrate temperature is raised to 350°C. While this is not a typical step in CdTe device fabrication, it will help us to understand the reactivity of Cu in the system.

Cu diffusion into CdTe from a back contact will be simulated by depositing approximately 10nm of Cu on top of the CdTe, annealing at 200°C in a N<sub>2</sub> atmosphere for 45 minutes, and etching the remaining Cu by an 18.5% HCl bath for 15 minutes.

CdS is the window material typically used in CdTe photovoltaics. It is conceivable that Cu diffuses all the way from the back contact to the CdTe/CdS junction or even in the CdS window causing a decrease in device efficiency. The experiments described above will, therefore, be repeated with CdS replacing CdTe.

Our preliminary results have shown that the local atomic and electronic structure of Cu impurities in CdTe on Quartz depends upon CdCl<sub>2</sub> treatment. However, based on these results, we cannot conclusively state that this difference is due to reaction with Cu in the CdTe or in the Quartz substrate. We plan a series of experiments that will allow us to identify the cause of this difference and to better understand the physics of Cu impurities in CdTe devices. The lack of Cu impurities in Kapton may make this an excellent substrate for CdTe devices, due to its flexibility and strength.

### 3.3 Soft-Hard Matter Interfaces

Interfaces and interactions between 'soft' and 'hard' materials Soft materials, typically composed of organic molecules, frequently have quite complex free-energy surfaces, and if so they tend to respond to very weak external stimuli by changing their structures and properties. Such materials are mechanically soft, but they may also be electrically, magnetically, optically or chemically soft. The result is that there is a wide variety of easily accessible phenomena to be explored in soft materials, and a large number of potential applications such as displays, optoelectronic devices, and chemical or biological sensors.

However, soft materials do not normally exist in their own separate world. Rather, many of the most intriguing or promising uses of soft materials are in conjunction with 'hard' (typically inorganic) materials. The process of molecular self-assembly at a solid-solution interface is an example of the use of 'hard' surfaces to nucleate soft materials. The reverse is possible as well: many living organisms use soft surfaces to nucleate hard materials. This allows these organisms to be hard-soft composites where the hard materials provide mechanical strength (skeletons) and, in some cases, sensing properties (for example, magnetite is used by some magnetotactic bacteria and perhaps by migrating birds to sense direction). The transport of 'hard' metal ions is a crucial biological function, carried out by soft organic molecules. In a thin film organic LED, the inorganic substrate serves to provide both mechanical strength and electrical contacts; hard surfaces help to align liquid crystals and polymers; and processes such as wetting, spreading and lubrication generally take place at hard-soft interfaces.

At MRCAT we perform a variety of studies of composite soft-hard systems, some of which are described below.

### 3.3.1 Studies of metal ion binding and mineral growth at Langmuir monolayers

Langmuir monolayers of carboxylic acids spread on aqueous solutions have been the object of intense investigation in the past decades.[27] Interest is driven by the desire for fundamental understanding of the interactions, as well as by the technological promise of transferred ("Langmuir-Blodgett" or LB) films. Langmuir systems are also studied as templates for oriented growth of crystals and as a model for the nucleation phase of biomineralization.[28]

Synchrotron grazing incidence diffraction (GID) experiments can be used to determine precise in-plane lattice parameters, chain tilts, and layer thicknesses of the organic monolayer. In addition, such studies have found that the presence of dissolved metal ions can lead to the creation of commensurate superstructures, sometimes with very large unit cells.[29]

To complement GID measurements, we will use grazing-incidence XAFS studies to explore the local structure about the metal ions in the area. As an example, Pb has been recently studied at MRCAT. The existence of a thin superlattice underneath long-chain fatty acid Langmuir monolayers spread over aqueous metal solutions was recently revealed by GID (see Figure ); these experiments determined the periodicity of the fatty-acid headgroups ( $a$ ,  $b$ ) and the commensurate superstructure ( $a'$ ,  $b'$ ), but could not give details on the type or structure of the adsorbed entities. In our recent work at the Pb  $L_{III}$  edge [30] we are able to show that Pb is covalently bound to the carboxylic headgroups and we observe Pb-Pb coordination at the interface. Analysis of the data based on measurements of aqueous Pb acetate and hydrolyzed Pb solutions concluded that Pb is most likely adsorbed as a hydrolysis trimer in which each Pb atom is bound to one carboxyl headgroup, with hydroxyl groups stabilizing the Pb triangle. This adsorption mechanism can explain the increased stiffness, largest area superlattice, largest surface potential change, and greatest monolayers compression produced by Pb in comparison studies with other divalent metals. We propose to continue this work in more systematic studies of pressure and pH, and with other metal / headgroup combinations, such as Cd and Ca.

When the subphase is a supersaturated solution of a metal salt, it is possible to nucleate not just an ultra thin layer but macroscopic crystals of various minerals, such as calcium carbonate (the most important biomineral), barium fluoride, etc. The Langmuir monolayer then serves as a model of the protein interfaces on which real biominerals grow from locally supersaturated aqueous environments. It has frequently been suggested [31] that the exquisite degree of structural control exercised by living organisms over biomineral growth is possible because there is a commensurate relationship between the organic and inorganic lattices, but this was first established by us using synchrotron diffraction (for  $BaF_2$  growth) only very recently.[32] While  $BaF_2$  is not a biological mineral, its growth under Langmuir monolayers is an example of 'biominimetic materials science'. Taking inspiration from nature, we attempt to grow epitaxial thin films and bulk crystals in ways somewhat analogous to what inorganic surface scientists do under UHV, but in "real world" conditions. We propose to extend these studies to a variety of inorganic crystal growth processes. Calcium carbonate (in the form of calcite or vaterite-calcite is the primary component of shells, vaterite of pearls) is of course a particularly interesting material; it is also easy to make supersaturated solutions of this material. Calcium phosphate, strontium fluoride and lead sulfide are also promising materials for these studies because preliminary experiments have been performed by others or because they are known to form stable supersaturated solutions.

We will use x-ray diffraction and XAFS to monitor the nucleation process in real time. At each point we will know what the organic lattice is, and we will simultaneously collect diffraction and/or XAFS data from the subphase. The two sets of diffraction peaks can be distinguished because the range of structures possible in fatty acid monolayers is now known, and also from the thickness of the scattering layer (indicated by rod scans). The XAFS is a useful complement to this because amorphous or extremely disordered crystalline phases can also be detected. We will seek to determine the role of surface functionality of the organic template by using acids, alcohols, amines, amides, etc.

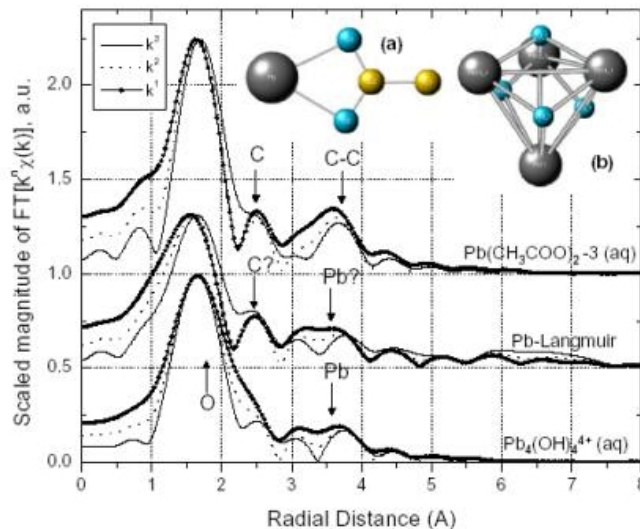


Figure 10: Fourier transform of XAFS of Pb bound to an acetate group, hydrolyzed Pb, and Pb adsorbed to the Langmuir monolayer. Magnitudes at different  $k$ -weightings for each sample are scaled to the first peak of the  $k^3$ -weighted transform. The relative magnitudes between samples at  $k^3$  are not adjusted. (a) bidentate-chelating binding of Pb by an acetate group - a standard for the analysis, (b)  $[\text{Pb}_3(\text{OH})_4]^{4+}$  hydrolysis complex, another standard. This and related data leads to the conclusion that metal is adsorbed as a hydrolysis complex, rather than as individual  $\text{Pb}^{2+}$  ions.

### 3.3.2 Metal adsorption to biological and mineral surfaces

Modeling the transport and fate of heavy metals in the environment is a central issue in environmental engineering and geochemistry. Interaction with diverse complexing media (minerals, biomass, etc.) must be considered under ambient conditions. In addition to more conventional chemical techniques, synchrotron radiation measurements have played an important role in this work.

An example of our recent work is a study of the adsorption of Cadmium to bacterial cell walls as a function of pH. Fluorescence XAFS was used to identify and quantify in-situ the adsorption channels of Cd to the isolated cell walls of a common groundwater bacterium, *Bacillus subtilis*. The results indicate that Cd binds predominantly to protonated phosphoryl ligands below pH 4.4, while at higher pH adsorption to carboxyl groups becomes increasingly important. At pH 7.8 we observe the activation of an additional binding site, which we tentatively ascribe to deprotonated phosphoryl ligands.[33]

Recently, we have begun investigating the simultaneous Cd adsorption onto the same *B. subtilis*, a Gram-positive aerobic bacterial species, and hydrous ferric oxide (HFO). We measure the bulk extent of adsorption, and we also use XAS to determine the distribution of the Cd in the mixed bacteria-mineral-water systems. We use equilibrium constants that characterize the Cd adsorption onto each sorbent to construct geochemical models of the adsorption behavior in the mixed systems, and we use the XAS results to test the accuracy of those models. We have been testing a range of systems, from bacteria-dominated adsorption to mineral-dominated adsorption.

In recently proposed work, we will investigate the universality of our work on *B. subtilis* by investigating other natural bacteria, including some that are Gram-negative and therefore have a rather different cell membrane. We propose to expose cultured bacterial consortia from different sampled settings to Cd, U, Pb, or Zn, and separate the exposed biomass for XAFS analysis. We will use the same approach taken in our previous studies of Cd and U binding onto *B. subtilis*. That is, we will also conduct XAFS analyses on

standard analogues that represent examples of binding between each metal and the likely binding site types on the bacterial surfaces. For example, metal-acetate solutions, of varying acetate compositions, will be analysed to model carboxyl binding on the bacterial surfaces. We will conduct the initial adsorption experiments to produce the biomass under different pH conditions to examine different binding mechanisms. The XAFS experiments will determine whether the mixed population of bacteria exhibits a simple or a complex binding behavior. Observation of simple behavior would strongly suggest that there is a common binding mechanism for all of the bacteria in the sample, providing a molecular-scale explanation for the universal adsorption behavior observed by Yee and Fein (2001).

This work will be generalized to include (1) gram negative bacteria, which have a much different cell membrane than the previously-studied Gram-positive *Bacillus subtilis*, and (2) different metal species, including U, Pb, or Zn. We also propose to extend our research of the effects of unicellular life-forms on metal speciation in the environment to compare the adsorption behaviors of algal and bacterial surfaces. Specifically, we propose to determine if algae, which have similar cell wall functional group types to bacteria, also exhibit similar binding properties and adsorption behaviors. Our approach will be similar to that of our early studies of metal-bacteria adsorption. We will conduct both bulk adsorption experiments with isolated single species of algae, and we will examine the biomass samples from these experiments using x-ray absorption spectroscopy. We will integrate the results from both of these types of experiments into surface complexation models of the metal-algal adsorption reactions. This work will also involve AFM and other surface-characterization techniques.

This work is part of a larger collaboration involving investigators from Notre Dame (Physics, Biology, and Civil Engineering and Geological Sciences Departments) and Argonne (Environmental Research and Chemistry Divisions). This collaboration has recently resulted in the formation of an Environmental Science Institute, funded jointly by NSF and DOE. Synchrotron radiation studies are a central part of this institute, with XAFS, x-ray reflectivity, and surface scattering used to augment other techniques.

### 3.3.3 Actinide fate and remediation

Several sites [34] around the world are contaminated with uranium due to uranium mining for the production of nuclear fuel, use in weapons, and the operation of the nuclear fuel cycle. Bioremediation using sulfur-reducing bacteria is being studied as an option for removal of uranium from these mining sites.[35] Many types of sulfate-reducing bacteria grow through anaerobic respiration.[36] The reduction or gain of electrons in sulfate-reducing bacteria results in the production of sulfide from sulfate, while the cytochromes on the bacteria are oxidized or lose electrons.

In some sulfate-reducing bacteria, the transfer of electrons can occur not only between bacteria and sulfate, but also between the bacteria and uranium. This microbial reduction of uranium, typically,  $U^{6+}$  going to  $U^{4+}$ , results in the conversion of a highly soluble form of uranium into an insoluble form. We believe that these microbes could be utilized to remove uranium from contaminated waters and soils. In most natural surface and ground waters, uranium(VI) is in the form of uranyl-carbonate complexes. The Uranyl-carbonate complexes usually result from various human activities that utilize uranium.[37] Studies have suggested that bacteria such as *Geobacter metallireducens* and *Desulfovibrio desulfuricans* can reduce the uranium(VI) that is in the uranyl-carbonate complexes. In these studies, uranium was observed to precipitate out from the solution. Therefore, microbial uranium reduction has the potential to remove solid uranium that was originally dispersed in a liquid. Microbial uranium(VI) reduction has several advantages as a remediation technique when compared to previously proposed treatments. These advantages include: the ability to precipitate uranium from uranium(VI)-carbonate complexes; the recovery of uranium in a highly concentrated and pure form; high uranium removal per amount of biomass; the potential to simultaneously treat organic contaminants and uranium by using the organic as an electron donor for uranium(VI) reduction; and the potential for in situ remediation of both ground and surface waters.[37]

Our collaborators at the University of Missouri, Columbia have a large body of research that suggests uranium is reduced by the sulfate-reducing bacteria, *Desulfovibrio desulfuricans*. *Desulfovibrio desulfuricans* is an anaerobic Gram-negative bacteria which contains c-type cytochromes and utilizes sulfate as an electron acceptor and lactate as an electron donor.[38] Their experiments have shown uranium(VI) is removed from a 1mM uranium assay with *Desulfovibrio desulfuricans* and an electron donor present.[39] Other experiments,[40] have shown that *Desulfovibrio desulfuricans* can effectively reduce uranium(VI) both at very high concentrations of 24mM and at relatively low concentrations of less than 50nM. However, no direct evidence exists that the end product of the reduction of uranium(VI) by sulfate-reducers is uranium(IV).

We propose to perform XAS measurements on U samples exposed to the sulfate-reducing bacteria, *Desulfovibrio desulfuricans* Strain G20, in order to verify that the reduction of uranium(VI) results in uranium(IV).

The first step towards understanding the bioreduction of uranium(VI) will be to prepare a bacteria culture. *Desulfovibrio desulfuricans* strain G20 will be grown in media containing lactate (60mM) as the primary electron donor and carbon source and sodium sulfate (50mM) as the terminal electron acceptor. 1:10 subcultures will be made from *Desulfovibrio desulfuricans* strain G20. These cultures will then be stored in a 35°C incubator in an anaerobic chamber.

A uranium assay will be done on the cells after approximately 24h of starting the culture during the logarithmic phase. A sodium bicarbonate solution, containing 2.5g of sodium bicarbonate/L of dH<sub>2</sub>O, will be used to dilute the Uranium acetate and to wash the cells. A 1M stock of sodium lactate and a 100mM stock of uranium acetate will also be prepared for the assay. For the assay, the pH of the sodium bicarbonate buffer will be adjusted to 7 and the uranium acetate stock solution should be diluted to a 1mM concentration using the buffer. The cells will be centrifuged for 10min at 5000 x g rpm then suspended in 1mL of buffer. The assay solution, containing 5mL of 1mM uranium acetate (electron acceptor), a 10mM concentration of sodium lactate (electron donor), and 0.5mg of whole cell protein, will then be stored in an anaerobic chamber. A control without an electron donor will also be prepared.

In order to determine that the concentration of uranium(VI) was disappearing from the assay solution, the Kinetic Phosphorescence Analyzer (KPA) will be used. Over time, 100(L samples will be withdrawn from the uranium assay to be analyzed with the KPA.

For XAS analysis at the MR-CAT, four samples will be prepared. A uranium(VI) oxide standard, a uranium(IV) oxide standard, the precipitate from the uranium assay, and the remnant solution will all be measured. The precipitate from the uranium sample will be collected by filtering out the solution of the uranium assay 48h after the addition of *Desulfovibrio desulfuricans*. The U L<sub>III</sub> XAS measurements will be performed in fluorescence geometry with the MR-CAT 13-element Ge Detector. The combination of the insertion device beamline and the multielement detector will be necessary to ensure high quality data from these low mass samples.

The goal of this research is simply to show that uranium(VI) is oxidized by *Desulfovibrio*. At low concentration, x-ray absorption spectroscopy is the best method for the determination of oxidation state of a material. We believe that we will be able to extend this work to other bacterial species that react with U, Pu, Np, and Am to develop methods of bioremediation and to better understand their fate in the environment.

### 3.3.4 Ordering of normal liquids at liquid-solid interfaces

Although there are significant positional correlations in bulk liquids, continuum hydrodynamics (where questions of molecular-scale structure are ignored) has been extremely successful in predicting many aspects of their dynamic behavior. On the other hand, it is known that the properties of liquids are different in pores or in the form of thin films, and such changes can only result from a change in the structure. The behavior of liquid near interfaces is of great relevance to industrial processes, lubrication, wetting, spreading (e.g. of

paints or oil spills), tertiary oil recovery, and many other applications, and insights gained from these studies may help design new materials and systems that enhance these applications. The results of these studies should also help us understand and control the behavior of liquids in other real-world confinement geometries, for example in porous minerals, in the form of droplets or suspensions, or within biological cells and capillaries.

Our recent studies at MRCAT [41, 42] provided the first x-ray diffraction evidence that normal (non-liquid-crystalline, nonmetallic, non-supercooled) liquids do form layers at a single interface; from the data we are able to extract quantitative density distributions, something that cannot be done with surface force measurements. (Surface force measurements also require two proximate interfaces and cannot be used to characterize isolated interfaces.) Such studies of internal interfaces requires making liquid films that are thin enough to allow the x-rays to pass through but thick enough not to introduce undesired Kiessig fringes, which mask the features of interest. We have developed the techniques for making stable films of suitable thickness. We would now like to extend these studies:

(a) Lateral order: We have already seen layering (order in the z-direction); however, especially at structured surfaces, it is reasonable to expect that the structure of the interfacial liquid will be modified. It has recently been reported that the local fivefold order in liquid lead is oriented at a silicon substrate.[43] We propose to investigate whether lateral ordering in liquids can be induced or controlled (and thus the properties of the liquid varied) by our choice of substrate or by temperature (supercooling may be particularly effective).

(b) Effect of shear: During lubrication, oil extraction from porous rock, etc., liquids are under high shear rates, and it cannot be assumed that their properties are the same as in bulk. Lateral surface force studies [44, 45] show that some liquids undergo shear thinning while others 'solidify' and show stick-slip behavior normally seen in crystalline material. What happens at a microscopic level is not well understood. We have already built an apparatus that allows us to study liquids under high shear rates.

### 3.3.5 Nanoscale iron phases in neurodegenerative diseases

Iron is essential to living organisms, however, disruption of normal iron metabolism and the accumulation of excess iron is a characteristic of several neurodegenerative diseases, such as Alzheimer's disease (AD), Parkinsons disease (PD), Progressive Supranuclear Palsy (PSP) and others.[46, 47, 48] For example, excess iron accumulation is known to occur in AD patients particularly in AD plaques [47] and total iron levels are elevated in the hippocampus, amygdala, nucleus basalis of Meynert and the cerebral cortex.[48, 49]

Though the association of anomalous concentrations of iron is well documented, particularly in Alzheimers and Parkinsons diseases, current methods for assaying iron in diseased tissue are ion specific, have poor spatial resolution and provide little reliable quantitative information.[50] For this reason, progress in determining the role of iron in neurodegenerative disease has been slow since this association was first reported by Goodman in 1953.[51]

In recent studies, however, some progress has been made in addressing these shortcomings in the histological analysis of iron in AD tissue. Smith and others [46, 52] have shown, using modified iron staining techniques, that redox-active iron is closely associated with AD plaques and neurofibrillary tangles. This work has demonstrated that lesion associated iron is distinct from iron sequestered in ferritin and has provided indirect evidence of the presence of Fe(II) in AD tissue. While this techniques does offer improvements in spatial resolution of iron distribution in AD tissue, identification of the iron compounds responsible for the anomalies or identification of concentrations of toxic Fe(II) is still not possible. As such, iron anomalies associated with neurodegenerative disease are not well characterized and the structural/molecular form of the excess iron in AD plaques and neurodegenerative tissue in general is not known.[53]

In the normally functioning human brain, as in the rest of the body, the primary mechanism for iron storage is in the core of the iron storage protein ferritin. Ferritin consists of a 12nm spherical protein cage made up of

24 subunits with a hollow ~8nm core in which iron is stored in the form ferrihydrite ( $5\text{Fe}_2\text{O}_3 \cdot 9\text{H}_2\text{O}$ ). All iron stored in ferrihydrite is in the ferric ( $\text{Fe}^{3+}$ ) state. Studies have shown that ferritin is approximately 10 times more abundant in the human brain than the iron transport protein, transferrin, which is responsible for the transport of iron across the blood brain barrier and through the cell membrane via transferrin receptors.[54]

As discussed previously, excess iron accumulation is associated with many neurodegenerative disorders and therefore likely plays an important role in disease initiation or progression. However, these elevated iron levels do not necessarily correlate with elevated levels of ferritin. In fact, in several regions of the brains of AD and PD patients, a reduction in transferrin, indicating reduced mobility and sequestration of iron, have been reported.[49, 55] This may be an indication of a breakdown in normal functioning of ferritin leading to increased iron loading in the ferrihydrite core or the sequestration of free iron. This view has very recently been supported by evidence that mutations in genes coding for H and L ferritin subunits leads to two types of neurodegenerative disease [neuroferritinopathy and Hallervorden-Spatz disease] without a corresponding increase in the total amount of ferritin.[56, 57]

Though increases in iron have been reported in neurodegenerative tissue without corresponding increases in ferritin, it is not clear in what form this excess iron exists. While the increase in iron may indicate increased iron loading in the ferritin core or the sequestration of free iron, another form of iron is likely present which could have significant consequences for disease progression and early detection biogenic magnetite ( $\text{Fe}_3\text{O}_4$ ) and maghemite ( $\text{Fe}_2\text{O}_3$  - an oxidation product of magnetite).[53, 58]

Magnetite is a ferrimagnetic iron oxide with alternating lattices of ferrous ( $\text{Fe}^{2+}$ ) and ferric iron which are antiferromagnetically coupled. This alternation of lattices and their corresponding differences in the number of unpaired electron spins give magnetite its strong magnetization, unlike the ferrihydrite core of ferritin (a superparamagnetic antiferromagnet). Magnetite and maghemite are the only magnetic iron compounds yet found in the human body and were first discovered in human brain tissue in 1992.[59] Although magnetite biomineralization is known to occur in a variety of organisms from bacteria to mammals,[60, 61, 62] this discovery proved controversial. Subsequent work has confirmed its presence in the human brain, though its origins and function are still unknown.[63, 64, 65]

Investigations of human brain tissue have demonstrated the probable presence of magnetite associated with plaque material in the hippocampus.[63] In addition, other investigations have provided preliminary evidence of magnetite in ferritin cores associated with paired helical filaments from AD tissue and bound to aberrant tau filaments in PSP [66] and in bulk samples of AD tissue.[59] This further highlights the importance of identifying not only the location of elevated levels of iron in affected tissue but also the nature of the iron compound present. This is particularly significant as magnetite provides a source of toxic  $\text{Fe}^{2+}$  and the relatively strong, local magnetic fields associated with it are very effective at generating free radicals via triplet state stabilization.[67] Experimental results also have demonstrated that iron-oxygen complexes may be a more effective catalyst for free radical damage in brain tissue than the Fenton reaction.[68] Most recently, the PI has presented preliminary evidence for an age-related increase in magnetite levels in the hippocampus of men.[69]

We recently have begun to develop a novel technique for the high-resolution examination of iron anomalies in neurodegenerative tissue using the MR-CAT beamline. There are three significant advantages to using synchrotron x-rays to study iron compounds in tissue sections:

It is possible to obtain information on not only the elements present in the tissue but also the atomic number, distance and co-ordination number of the elements in question via XAFS.

Using XANES, information on the vacant orbitals, electronic configuration and (via analysis of the absolute position of the iron absorption edge) information about the oxidation state of the absorbing atom (i.e. ferric or ferrous iron).

The technique is automated and scaleable, allowing large areas of tissue to be scanned at low resolution then moving in to scan anomalous areas at high resolution (~ 5 mm pixel size).

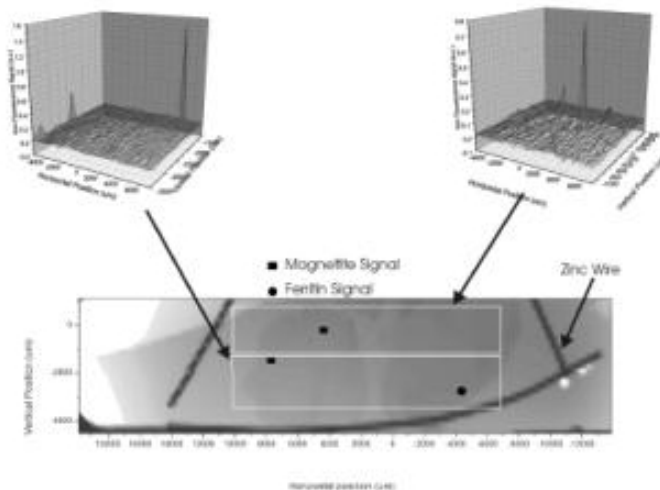


Figure 11: Iron edge scan of avian brain tissue section. The lower image is an x-ray transmission image and the two irregular shadows contained within the grid lines represent the tissue sections. The two top images represent the intensity of the iron fluorescence as a function of scan position (the rastered scan lines are visible).

This technique will enable high-resolution mapping of the distribution of various iron compounds in tissue samples. This information will be combined with other microscopy techniques as described in the proposal and used to identify the anomalies and map them to specific cells and structures in the tissue. This represents a major breakthrough in the study of iron in the brain and the role of iron in neurodegenerative disorders.

Ultimately, we propose to examine the magnetic properties of neurodegenerative tissue in combination with XAFS and XANES in order to understand whether changes in brain iron levels correspond to changes in the magnetic properties of the iron compounds present. The primary significance of this part of the proposed work may lie in the development of Magnetic Resonance Imaging (MRI)-based mechanisms for early detection of neurodegenerative disease.

High-resolution mapping of iron anomalies and nanoscale iron biominerals in brain tissue has proven difficult up to now.[50, 58] Our initial attempts to make elemental maps of samples using Transmission Electron Microscopy (TEM) combined with Electron Energy Loss Spectroscopy (EELS) imaging holds some promise, however, the equipment for this work is prone to malfunction and only very small areas of a tissue slice may be examined in each session (generally only a few  $\text{mm}^2$  within a reasonable measurement time). Size restrictions again apply to Atomic Force/Magnetic Force Microscopy (AF/MFM) investigations of tissue samples only very small areas can be scanned within a reasonable time-frame. This creates a major problem for imaging and mapping iron at high-resolution over larger areas such as those presented by histological slides (areas on the order of a few  $\text{cm}^2$ ).

A pilot project, funded by the University of Florida Opportunity Fund, was begun in December, 1999 to investigate the possibility of imaging, mapping and characterizing iron in biological samples using high-energy x-ray scanning the Advanced Photon Source (APS) synchrotron at Argonne National Laboratories (ANL). The main goal of this project was to examine the feasibility of using synchrotron x-rays as a method of not only mapping large areas in tissue sections at high resolution but also determining the structural phase of any iron anomalies detected.

This project has resulted in the successful development of tissue preparation and handling methods for synchrotron analysis and has provided preliminary results that demonstrate the viability of these techniques for iron mapping in biological samples. Initial studies of avian (pigeon) brain tissue indicate that iron anomalies

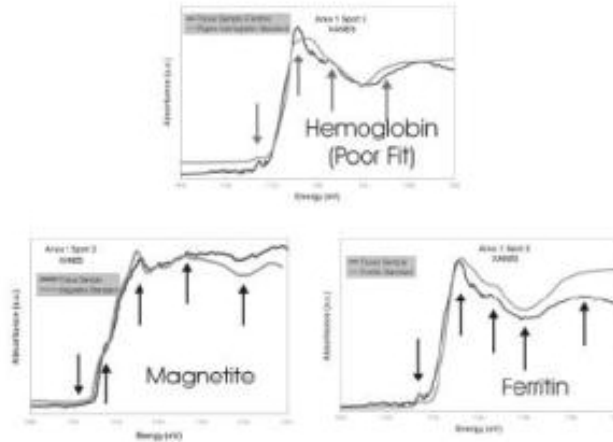


Figure 12: Comparison of XANES near-edge oscillations for magnetite, ferritin and hemoglobin standards with iron anomalies seen in the upper region scans from Figure 11.

can be located and characterized in tissue sections via our synchrotron scanning methods. Figure 11 shows an iron edge area scan of avian brain tissue from the mid-brain region in which three major anomalous iron peaks can be seen. XANES scans were analyzed for each of the three major anomalies seen (Figure 12).

Based on comparison with ferritin, hemoglobin and synthetic magnetite standards, two of the anomalies were determined to arise from magnetite and one from ferritin (Figures 11 and 12). The two insets represent the iron fluorescence signal as a function of position within the two marked portions of the tissue sample. The lower image is an x-ray transmission image obtained from the same data set used to generate the x-ray fluorescence maps.

The dark bands observed in Figure 11 are zinc wires which were deposited on the thermoplastic mountings using photolithography. The wires will provide a grid system for location of the microscale anomalies within the low-magnification image of the tissue. Using this grid system, the same tissue samples can be imaged, either before or after synchrotron scanning, using a variety of imaging techniques (e.g. confocal microscopy, light microscopy, electron microscopy and AF/MFM). Each technique provides unique information on the anomaly and its associated tissue and cellular structures. The anomalies can be observed using techniques operating at different magnifications by using the grid system to home in on the precise location of the microscale anomaly in a relatively large tissue section (on the order of a few  $\text{cm}^2$ ). These images can then be overlain using the grid system for orientation to create a composite image that contains information obtained from each imaging technique. This novel method should provide a powerful tool for multi-modal image analysis of the anomalies and surrounding tissue resulting in a better understanding of the form of iron present and its association with tissue and cellular structures. Once identified and mapped, a photolithographed zinc grid system can be used to locate the anomalies using other imaging techniques, such as light, confocal, electron and atomic/magnetic force microscopy. Each imaging technique provides unique information on the anomaly, which can then be aggregated into a composite image using the grid system.

The techniques developed using avian tissue models will be applied to high-resolution iron mapping of human samples of neurodegenerative tissue and age-matched, non-pathologic controls. This technique represents a major breakthrough in the study of the role of iron in the brain and will enable, for the first time, detailed investigation on a cellular level of the structure of iron anomalies associated with neurodegenerative diseases. This information will be used to make greatly improved assessments of the origins and role of anomalous iron in neurodegenerative disease.

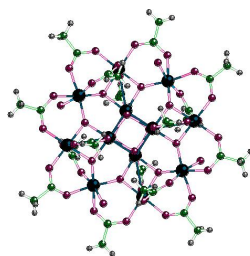


Figure 13: The neutral  $[\text{Mn}_{12}\text{O}_{12}(\text{COOCH}_3)_{16}(\text{H}_2\text{O})_4] \cdot 2\text{CH}_3\text{CH} \cdot 4\text{H}_2\text{O}$  cluster. Note the cubane-like structure in the center of the molecule. Mn atoms are black, C atoms are green, O atoms are purple, and H atoms are gray.

### 3.4 Physical Chemistry

#### 3.4.1 Manganese and Vanadium molecular clusters

Some of the most interesting materials being synthesized currently are composed of metal oxide cluster building blocks. Such materials offer the opportunity to study the effects of electron transfer caused by changing ligands or different arrangements of the clusters in extended frameworks. X-ray absorption studies, coupled to computational modelling provide an ideal way to study the electronic and structural properties of these kinds of systems. In particular, we are working on molecular magnets based on the  $[\text{Mn}_{12}\text{O}_{12}(\text{COOR})_{16}(\text{H}_2\text{O})_4]$  molecule and catalytic materials such as  $[\text{Co}_3(\text{H}_2\text{O})_{12}\text{V}_{18}\text{O}_{42}(\text{SO}_4)] \cdot 24\text{H}_2\text{O}$ .

Nanometer scale magnets made from inorganic building blocks with backbones of organic molecules have emerged as a new class of materials. The first molecular compound to be identified as a magnet was  $\text{Mn}_{12}\text{Ac}$ ,  $\text{Mn}_{12}\text{O}_{12}(\text{COOR})_{16}(\text{H}_2\text{O})_4$ . [88, 89] This class of magnetic molecules has an organic backbone that can be modified to give the magnet a different chemical functionality (see Figure 13). Early attempts at chemical functionalization have changed the chemical solubility of the nanomagnets [90] and have facilitated the formation of Langmuir-Blodgett films. [91] The ability to change the chemical properties of the magnets may allow for the preparation of novel inductors, high-density storage devices, and even liquid magnets. However, changing the ligands (i.e. chemical functionality) also modifies the electronic structure of the manganese atoms; thus changing the magnetic properties of the cluster. By studying the effect that different ligands have on the manganese atoms, we believe that we can provide guidance on what molecules will likely be the best molecular magnets.

Transition metal oxides catalyze many important industrial chemical transformations. [95] For example, vanadium oxide supported on titanium oxide is a commercial (DeNOx) catalyst for the removal of the environmentally detrimental oxides of nitrogen - NOx (mainly NO and NO<sub>2</sub>) - from the exhaust of automobile engines and flue gas streams of stationary industrial establishments by selective catalytic reduction (SCR) of NOx gases to N<sub>2</sub> and H<sub>2</sub>O by NH<sub>3</sub>. [96] However, the mechanism of interactions of the catalytic (transition metal oxide) surfaces with substrate molecules is, at best, enigmatic due mainly to the complex nature of these poorly characterized surfaces that are inaccessible to many physico-chemical techniques. [95] The suitability of the currently employed catalysts is determined empirically with practically little or no possibility of improvements in their performance.

Transition metal oxide clusters [100, 101, 102, 103, 104] or polyoxometalates of vanadium, molybdenum, and tungsten and their derivatives provide an exciting opportunity to develop rationalized approach for preparing new generation of materials with desired properties. Our collaborator (M.I. Khan, Illinois Institute of Technology) has synthesized and characterized a new class of nanostructured materials of general formulation:  $(\text{Cation})_m[\text{M}_3\text{V}_{18}\text{H}_a\text{O}_{42}(\text{XO}_4)(\text{H}_2\text{O})_{12}]_n \cdot \text{cH}_2\text{O}$ . (Cation=Li, Na, NH<sup>4+</sup>, etc.; m=0-6; M=Mn, Fe, Co,

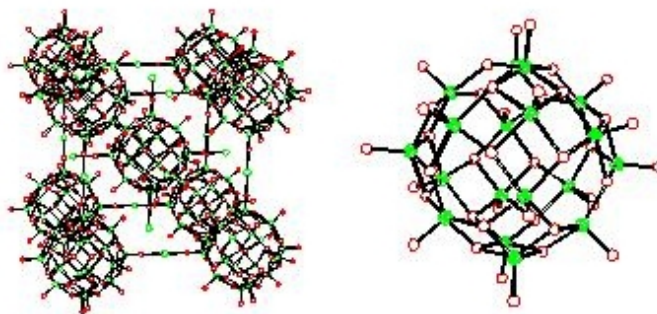


Figure 14: A view of the new material containing 3-D arrays (left) of the constituent  $\{V_{18}O_{42}(XO_4)\}$  cluster (right).

etc.;  $a=0-6$ ;  $X=V, S, Cl, \text{ etc.}$ ;  $n=0-6$ ). The structure of a prototypical compound,  $[Fe_3(H_2O)_{12}V_{18}O_{42}(XO_4)] \cdot 24H_2O$ , of this series of solids is shown in Figure 14.

The highly symmetrical nanostructured solid  $[Fe_3(H_2O)_{12}V_{18}O_{42}(XO_4)] \cdot 24H_2O$  contains well-ordered three-dimensional arrays of  $\{V_{18}O_{42}(XO_4)\}$  nanoparticles interlinked by bridging  $\{Fe(H_2O)_4\}$  linking groups.

Besides their interesting structural, electronic, and ion exchange properties, this new class of solids may have potential applications in heterogeneous catalysis. Preliminary studies on  $[Co_3(H_2O)_{12}V_{18}O_{42}(XO_4)] \cdot 24H_2O$  indicate that the new material is an oxidation catalyst which catalyzes the selective oxidation of olefins, especially of the propene over a wide range of temperature.

In 3d transition elements such as V and Mn, the absorption at the K-edge serves as a measure of the unoccupied d-states (pre-edge quadrupole transitions) and as fingerprint of the nominal charge transfer at the absorbing atom (chemical shift and edge features). We have obtained initial XANES data on the unoccupied electronic structure of  $[Mn_{12}O_{12}(COOCH_3)_{16}(H_2O)_4] \cdot 2CH_3CH_2 \cdot 4H_2O$  and  $(PPh_4)_2[Mn_{12}O_{12}(COOCHCl_2)_{16}(H_2O)_4] \cdot 4CH_2Cl_2 \cdot H_2O$ . The spectra of the  $Mn_{12}O_{12}$  cluster were significantly different when complexed with different ligands. In this case, two Mn(III) ions in the outer ring were reduced by the electron donating ( $PPh_4$ ) group. Using the known structure of the  $Mn_{12}O_{12}$  cluster and the ligands, we have used the FEFF 8 [21] program to self-consistently calculate the XANES spectrum of the Mn atoms and the charge transfer on each atom in the cluster. The results of the calculations (see Figure 15) show a remarkable agreement with the measured XANES spectra and the charge transfer by other calculations.[87]

We have also begun preliminary XANES measurements on vanadium oxide complexes, including  $\{V_{18}O_{42}\}$  based materials. The edge structures in Figure 16 clearly show the subtle effects of changing an anion located far away from the V (red and green curves) and the more visible changes obtained when there is a vanadium dimer (blue curve). These results are comparable to those we have obtained on  $\{Mn_{12}O_{12}(COOR)_{16}(H_2O)_4\}$  based materials described above.[92, 118, 119] There are a number of known V-based single molecule magnets in the literature,[121, 122] it is likely that with suitable charge transfer, we will be able to observe similar properties in the  $\{V_{18}O_{42}\}$  based materials. These electronic structure measurements and calculations are proving to be a powerful predictive tool for elucidating the properties of the magnetic molecules. We plan to extend these results by further XANES measurements and calculations on molecules with different ligands.

The first measurements we have conducted on  $Mn_{12}Ac$  and its derivatives were synthesized by others [92] and transported to MR-CAT. This resulted in a time delay between measurement and synthesis. In order to reduce the time between synthesis and measurement we recently developed the capability to synthesize  $Mn_{12}Ac$  and its derivatives at IIT. To date, we have prepared  $Mn_{12}Ac$  and a stearate derivative.[93] In addition to the XANES measurements, which only indirectly probe the magnetic state of the Mn atoms, we

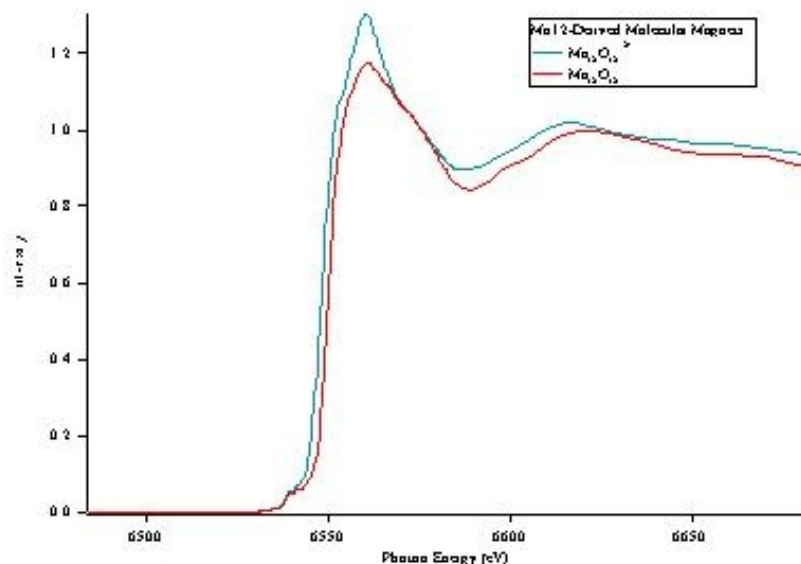


Figure 15: A full multiple scattering XANES calculation utilizing the quadrupole approximation is compared to our data from the neutral cluster. Good agreement was obtained in the peak positions. The shift in the pre-edge features is a known artifact of the calculation.[94]

plan to extend our studies to X-ray Magnetic Circular Dichroism (XMCD) measurements. We are collaborating with Klaus Attenkofer of Argonne National Laboratory to build an x-ray quarter wave plate which can be installed on the MR-CAT beamline. The MR-CAT beamline is particularly well-suited to these studies because of its design as a spectroscopy beamline.

In addition, we plan to study the catalytic properties of materials such as  $[\text{Co}_3(\text{H}_2\text{O})_{12}\text{V}_{18}\text{O}_{42}(\text{XO}_4)] \cdot 24\text{H}_2\text{O}$  using *in-situ* XANES and XAFS. The structure near the absorption edge serves as a measure of the unoccupied d-states and as fingerprint of the nominal valence state of the absorbing atom (V or Co in this material). By studying the changes in the near edge absorption spectra as a function of the reaction conditions, it will be possible to correlate improved catalytic properties with the electronic state of the key metal atoms in the structure. The XAFS spectra will additionally provide information about the reactions which occur at the metal atom sites. An example of this technique is the study of  $\text{O}_2$  reaction with alumina-supported (Co)MoS<sub>2</sub> catalysts.[116] The difference in spectra before and after exposure to oxygen at 20°C and 100°C show that displaces S about Co and then Mo (at the two temperatures, respectively). This kind of information is not easy to obtain with other means and is important in understanding the catalytic processes as well as the conditions under which the catalyst will be active or deactivated.

### 3.4.2 Technetium Radiopharmaceuticals

The nuclear power industry has spawned a number of successful spin-off technologies. At MR-CAT, we have been involved in efforts to improve and understand radiopharmaceuticals. At the present time, more than seventy-five percent of routine nuclear medicine diagnostic procedures use technetium-99m (<sup>99m</sup>Tc).[78] This isotope is an ideal imaging agent in that it decays with a half-life of 6.03 hours to <sup>99</sup>Tc primarily by the emission of a 140 KeV gamma-ray. The gamma-ray is high enough in energy to readily penetrate (escape) tissue but low enough in energy to be absorbed with very high efficiency by the thin thallium-

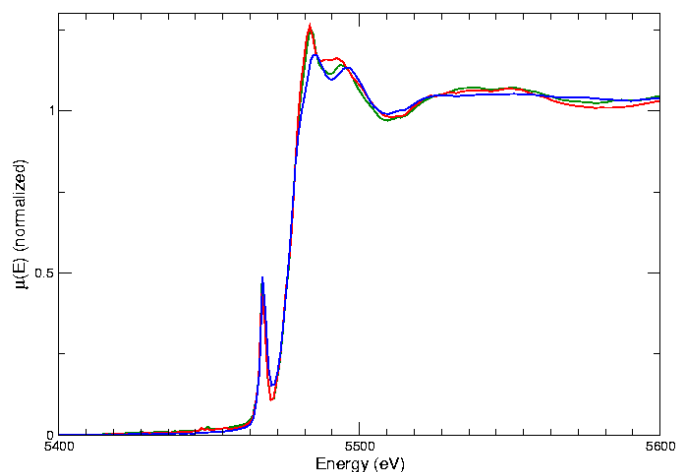


Figure 16: Vanadium absorption edge of three V-O complexes;  $[\text{VO}(\text{SO}_4)(\text{H}_2\text{O})_4]\text{SO}_4[\text{H}_2\text{N}(\text{CH}_2\text{CH}_2)_2\text{NH}_2]$  (red);  $[\text{VO}(\text{SO}_4)(\text{H}_2\text{O})_4]\text{SO}_4[\text{HN}(\text{CH}_2\text{CH}_2)_3\text{NH}]$  (green); and  $[\text{V}_2\text{O}_2(\text{OH})_2(\text{SO}_4)(\text{C}_{10}\text{H}_8\text{N}_2)_2]$  (blue).

doped, sodium iodide, single-crystal slabs used in the various nuclear medicine imaging cameras. Although other radioisotope generator systems offer some real advantages over the  $^{99}\text{Mo}$ - $^{99m}\text{Tc}$  generator, the use of  $^{99m}\text{Tc}$  is still increasing.

Even though  $^{99m}\text{Tc}$  is by far the most widely used radioisotope in nuclear medicine, much about its chemistry remains unknown. Technetium is a second-row transition metal and can assume any oxidation state from +7 to 0. It resembles manganese to a limited extent and rhenium to a much greater extent. In its compounds, it exhibits coordination numbers from 4 to 9 and their crystal structures show great variety. Complexities in the chemistry, especially in aqueous solution, make it difficult to assign an overall role to its behavior in medically useful radiopharmaceuticals as one might do in the case of much better understood elements like nickel and cobalt. In water, many of its compounds hydrolyze, polymerize, and become colloidal.[79]

Our  $^{99m}\text{Tc}$  work has two thrust areas, the structural determination of radiopharmaceuticals and the determination of radiopharmaceutical interactions in the body. Only recently has the FDA required structural information for new imaging agents.[80] The structures of three of the most widely used  $^{99m}\text{Tc}$  imaging agents are still not known: Tc-99m Pentetate used for kidney and brain imaging and assessment of renal perfusion; Tc-99m Medronate used as a bone imaging agent to delineate areas of altered osteogenesis; and Tc-99m Sodium Phosphates used both for bone and myocardial imaging and blood pool and gastrointestinal imaging. At the same time, very little is known about the metabolism and the ultimate fate of the various  $^{99m}\text{Tc}$ -containing radiopharmaceuticals that are injected. The ultimate aim of this proposed work is to use XAS to characterize the chemistry and structure of technetium compounds and their metabolites at the low concentrations in which they occur in the radiopharmaceutical formulations and in blood, tissue and urine.

We have recently completed our first set of XAS measurements on a series of "standard"  $^{99}\text{Tc}$  compounds at MR-CAT's 10-ID undulator beamline. Technetium-99 was used because of its much longer half-life (210,000 years) and corresponding lower specific activity. This work allowed us to accumulate spectra for technetium in numerous oxidation states (+4, +5, +7) with a variety of ligands (oxygen, chlorine, nitrogen, and carbonyl). The results from this preliminary run indicate that we will be able to investigate the chemistry and structure of technetium compounds with only nanomoles of  $^{99}\text{Tc}$ . This is the exact amount of technetium that is eluted from a generator and incorporated into a radiopharmaceutical with a standard kit.

Figure 17 shows the Tc K-edge x-ray absorption spectra from a series of Tc standards where Tc occupies oxidation states of (IV - VII). These spectra are very interesting from a chemical physics standpoint as there is no evident trend of edge position vs. oxidation state. These measurements confirm the early measurements

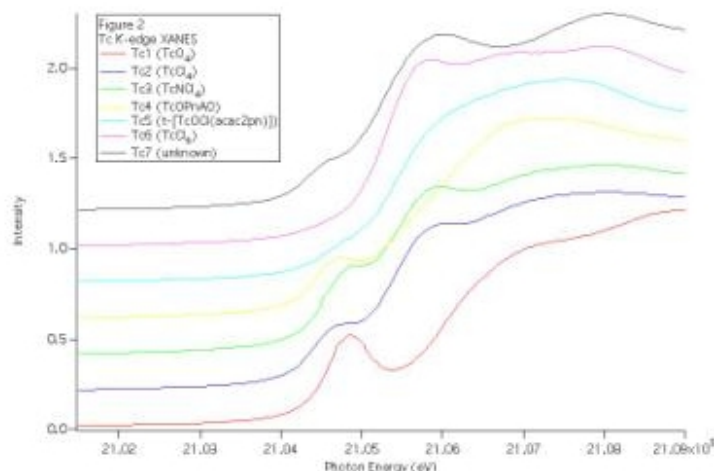


Figure 17: Tc K-edge x-ray absorption spectra from standard Tc compounds are shown.

of Shuh, et al.[81] This suggests that final state effects play a very large role in the absorption of x-rays in Tc compounds. Final state effects occur as the remaining electrons rearrange to lower the energy of the system as a photoelectron is ejected. While this complicates the identification of samples with unknown oxidation state, theoretical modeling with the x-ray absorption analysis program FEFF [21] should allow us to understand these systems.

Fortunately, the structural information in the XAS spectra from the series of Tc standards is much easier to understand. The peaks in Figure 18, the R-space transform of the EXAFS data, are related to the distances between the absorbing Tc atom and its neighbors atoms formed with technetium. Analysis of these spectra, have allowed us to "fingerprint" certain bond lengths in Tc compounds. For example, we have observed Tc-O bond lengths of 1.70 ( 0.02 Å and Tc-Cl bond lengths of 2.35 ( 0.02 Å in TcNCl<sub>4</sub>, TcOCl<sub>4</sub>, and TcCl<sub>6</sub>, for example, have similar Tc-Cl distances. This Tc-Cl distance appears as the peak at approximately 2 Å in the spectra labeled Tc2, Tc3, and Tc6 in Figure 18. We concluded that the EXAFS method is a valid technique for determining local crystal structures of the Tc compounds.

We now propose to improve our understanding of Tc radiopharmaceuticals through the use of Tc K-edge XAS. Our first goal will be to determine the local structure of currently used Tc radiopharmaceuticals (Tc pentetate and Tc medronate) that have unknown crystal structure due to an inability to crystallize these compounds. Our second goal will be to determine the structure of Tc compounds in blood, tissue, and urine samples. It is in these environments that XAS really excels as a structural tool as x-ray diffraction provides little data due to the lack of long-range order.

Local Structure of Tc Compounds - Tc pentetate and Tc medronate samples will be performed in the following manner. Initially, technetium will be eluted from a Mo-Tc generator and incorporated into a radiopharmaceutical using the standard methodology.[82] Approximately 1 microgram of <sup>99m</sup>Tc radiopharmaceutical in aqueous solution will be encapsulated in a standard radioactive liquid sample holder. These samples will be transported to MR-CAT following standard DOT rules. The Tc K-edge XAS spectra will be measured in fluorescence geometry with the MR-CAT 13-element Ge Detector. The low quantity of material in these samples necessitates the combined use of undulator radiation and multielement detector to ensure good measurement statistics. Both oxidation state and local geometric structure of the Tc absorbers will be determined through theoretical modeling with the program, FEFF.[21]

Local Structure of Tc in Tissue - Here our interest is in the determination of Tc interactions with blood,

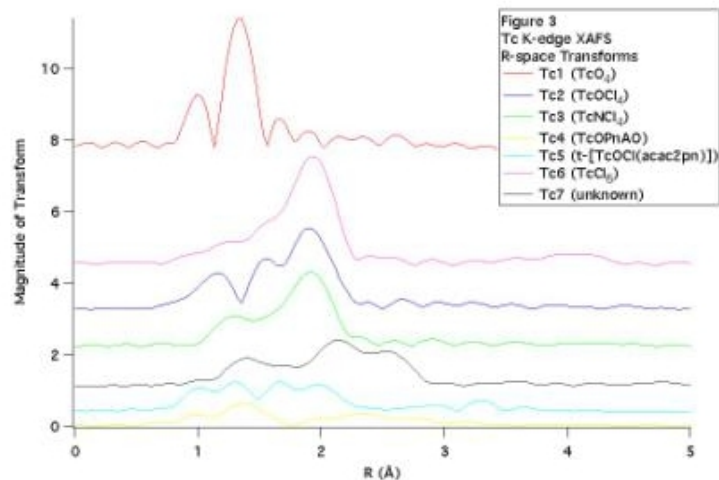


Figure 18: R-space Transforms of Tc K-edge x-ray absorption spectra from standard Tc compounds are shown.

tissue, and urine. This will allow us to better understand the mechanistic of radiopharmaceutical/tissue interactions in the body. In this case, the XAS measurements at MR-CAT will be exactly as above. The only difference is that double blind clinical samples from actual patients undergoing treatment with the  $^{99m}\text{Tc}$  radiopharmaceuticals will be studied.

Currently, XAS is the only technique that can provide both chemical state and chemical structure information at the low materials concentrations present in bodily tissue and fluids. We plan to perform simple XAS measurements to characterize the chemistry and structure of technetium radiopharmaceutical formulations in blood, tissue and urine. We believe that we will demonstrate that XAS can be used as a tool by drug researchers seeking to produce new pharmaceuticals by determining actual chemical pathways in the body.

### 3.4.3 GIDX-ray Diffraction Of Polymerizing Langmuir Monolayers

Self-assembled monolayers (SAMs) have received wide acceptance as a means of modifying surface properties of many materials. The convenience and efficiency of SAMs have led to their application in surface patterning,[123, 124] molecular lubrication,[125] and in corrosion prevention,[126] to cite a few examples. Commonly used SAM systems are derived from amphiphilic compounds of alkanethiols, fatty acids, and alkylsilanes.[127] Unlike alkanethiols where the interactions are limited to substrate-molecule and van der Waals chain-chain interactions, alkylsilanes are capable of forming chemical bonds with each other as well as the surface, thus adding additional potential film growth mechanisms at substrates. In addition to their application in SAMs, alkylsilane chemistry is at the heart of much of the explosive growth in mesotextured materials.

SAM films resulting from alkylsilanes are well-known to be semi-crystalline, with alkyl chains oriented normal to the surface. The mechanism of lateral growth of these SAMs at solids has been debated over the years, with either island growth, as suggested by Dutta et al. [128] and others [129, 130, 131, 132, 133, 134] or homogeneous growth [135, 136] modes suggested in the literature.

The lateral film growth of alkylsilanes can be effectively isolated from the influence of a solid substrate in a Langmuir trough, where the surface pressure imposed by displacing the barrier can be conveniently controlled to vary the surface density and energy involved in the chemisorption of the silane molecules to the water substrate.[137] Under these conditions, the intermolecular chemistry intrinsic to the alkylsilane

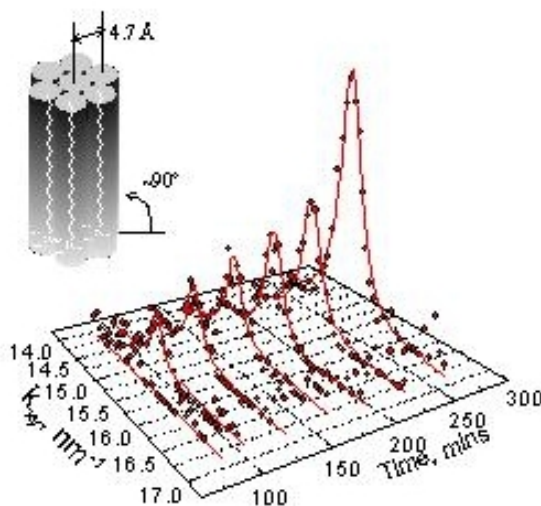


Figure 19:

molecules may be investigated, as the water surface is fluid and will not pin reactive species to a given location at the substrate. The positional ordering in a floating Langmuir monolayer more closely reflects the van der Waals interchain interaction and the intrinsic lateral chemical bonding of the silane headgroups than such a film self-adsorbed to a solid. Additionally, vertical film growth modes are impossible.

Since the first reported GIXD studies at the air-water interface by Dutta[137, 138][138] and Kjaer,[139] the focus of most synchrotron monolayer studies has been in situ investigations of compression and temperature effects on structure. We are interested in x-ray studies of time-dependent effects in floating monolayers. The main problem is the weakness of the scattered signal, which imposes the need for 3<sup>rd</sup> generation x-ray beamlines so that the data acquisition can be done in the required time and at an adequate resolution. To this end, we constructed and commissioned a general use GID Langmuir trough, which is mounted on a piezo-vibration table within the center of the Huber 8 circle goniometer at the MRCAT undulator beamline.

Many groups, including ourselves, have investigated the reactions of alkylsilanes in Langmuir monolayers.[140, 141, 142, 143, 144] In particular, 2D viscometry has shown that a crosslinked network results from the reaction of n-octadecyltrimethoxysilane [OTMS,  $\text{CH}_3(\text{CH}_2)_{17}\text{Si}(\text{OCH}_3)_3$ ] monolayers under acidic conditions. The kinetics of this polymerization process and the evolution of the resulting mechanical properties with extent of reaction are reproducible. Figure 19 above shows that standard Langmuir trough monolayer techniques coupled with GID at the MRCAT beamline enables sufficient time-resolution to follow structural changes induced by a polymerization reaction.[142] We have also reported that a nucleation-type growth precedes the 2D gelation of the material.

Ongoing and planned studies take further advantage of the possible capabilities of the beamline. For instance, the data in Figure 20 come from quickscan runs, where diffraction peaks can be resolved at faster than one scan per minute. These more rapid experiments allowed us to observe a systematic evolution of the peak position and correlation length (from FWHM data) early in the polymerization reaction consistent with hexatic ordering.

A second class of experiments probes the kinetics of how crystalline domains of a crosslinked polysilane monolayer dissociates. To accomplish this, a crosslinked monolayer is formed at constant pressure and the lateral pressure is instantaneously reduced. The accompanying plot shows an example of how rapid diffraction scans can elucidate the dissociation process. By a series of protocols, we hope to identify signatures of the underlying hydrolysis and condensation reactions and better control the overall reaction.

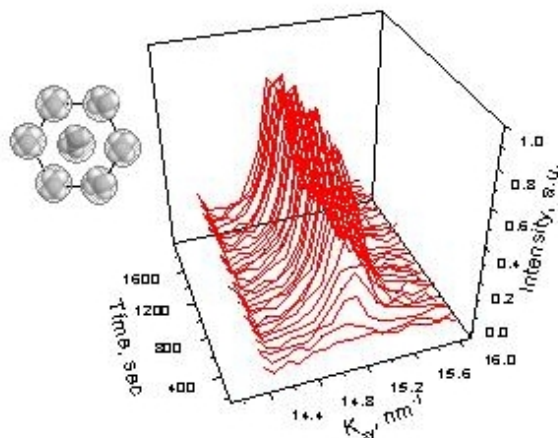


Figure 20:

## 4 Institutional Description

The Materials Research Collaborative Access Team was initially organized in 1991 to develop a materials research oriented sector at the Advanced Photon Source (APS). Over the past seven years, the team has added new institutional members whose research expertise has broadened the MRCAT scientific focus as described in Section 3. The current institutional members of MRCAT are Illinois Institute of Technology (IIT), Northwestern University (NU), University of Florida (UF), University for Notre Dame (UND), the Chemical Technology and Environmental Research Divisions of Argonne National Laboratory (CMT/ER), and BP-Amoco Corporation. Each of these institutions has a representative on the Executive Committee which makes overall financial and policy decisions. Executive Committee members also take on management roles within MRCAT. These include CAT Director (B. Bunker, UND), Associate CAT Director (C. Segre, IIT), Chief Financial Officer (V. Maroni, ANL/CMT), and Publications Coordinator (P. Dutta, NU). Executive Committee meetings are held at least six times per year to discuss how the project is being managed. In addition, the APS has recently instituted a thorough sector review procedure which will examine the quality of MR-CAT scientific output on a triennial schedule. This will provide MR-CAT with the opportunity to revisit its mission and change scientific direction over time.

## 5 Budget Justification

### 5.1 Staff Salaries

The MRCAT Staff is responsible for the day-to-day maintenance and operation of the facility, design and procurement or construction of new equipment for the beamline, training of new users, scheduling of beam time and overall safety. The staff members are detailed below with a more complete delineation of their responsibilities. All full-time scientific and engineering staff participate in user support during experimental runs. MRCAT also makes use of the resources of the CSRRI at IIT. We have obtained support from the CSRRI in design review and fabrication of mechanical systems, crystal optics and other beamline components as well as support for commissioning studies. The presence of the CSRRI permits us to have a somewhat smaller on-site staff than is ideal for an operation of our size and it has enabled us to be an integral part of innovations in beamline optics such as the new cryocrystal design and fluorescence EXAFS detector.

*Project Manager* It has been demonstrated that successful Collaborative Access Teams at the APS have an on-site Director or Associate Director who participates materially in the management of day-to-day activities of the CAT. For MRCAT, this role is fulfilled by the PI, C. Segre, of IIT. His responsibilities include calling and running staff meetings, making technical and procurement decisions within the guidelines set by the Executive Committee, final say in scheduling and beam time accounting, and Safety Coordinator. Dr. Segre is Professor of Physics at IIT and is the Associate Dean for Research in the Armour College. This last position permits him to spend as much time as necessary at APS (usually 2 full days per week).

*Scientists* (2 FTE) Duties include maintenance of beamline, development of new scientific equipment or capabilities and acting as scientific collaborators for users from the participating institutions. Each scientist is also responsible for user training and safety oversight during experimental runs. Scientists are involved in the decision-making for operations and are encouraged to conduct their own research activities, either independently or in collaboration with beamline users.

*Beamline Scientist* (1 FTE) This individual will be responsible for the final design and assembly of the bending magnet First Optical Enclosure experimental station. MR-CAT members have made a considerable investment in the bending magnet line to this point. We have an FOE with a lightly shielded second compartment for experimental equipment, a spectroscopy table, a Huber 4-circle goniometer, a complete set of electronic and motor control equipment to instrument the line, a channel-cut monochromator and slits and a design for a beam stop and mask. This scientist will complete the ray tracing and final design report and assemble and commission this experimental station.

*Software Specialist* (0.8 FTE) The beamline control systems are critical for users to efficiently perform their experiments. Just like the hardware, the software side of the beamline is constantly being upgraded because of new experimental techniques and a need for improved user interfaces. While we are continuing to share our Software Specialist with IMCA-CAT (since we both use the same beamline control system- MX [146]), the varied nature of the experimental techniques available at the MR-CAT facility demands a continual software development and we expect to have a need for 80% of this person's time.

*Administrative Assistant* (0.5 FTE) This person is responsible for maintaining day-to-day financial record, provide support for the beam time allocation process and maintain the MRCAT Web Page. With the varied funding sources supporting MR-CAT, good financial record keeping is essential and must be handled by a dedicated staff member. As we continue to increase the numbers of General Users who use the MR-CAT facilities, this person will serve as an initial, administrative contact in lieu of the Project Manager.

## 5.2 Operational Costs

The total expenditures, including staff salaries are in the range of \$4,000 per day of available beam. The MRCAT member institutions have made a commitment to fund about 50% of these direct operating costs for the next three years. **{MORE NEEDS TO BE ADDED HERE}**

## 6 Biographical Sketches

### Carlo U. Segre, PI

Physics Division  
Illinois Institute of Technology  
3101 S. Dearborn Chicago, IL 60616  
Voice: (312) 567-3498; Fax: (312) 567-3396  
e-mail: Carlo.Segre@iit.edu  
Ph.D. University of California, San Diego, 1981

#### Post Ph.D. Activities and Honors

Associate Dean for Research of Armour College, IIT 2002-  
Professor of Physics, IIT, 2001-  
Assoc. Director, Materials Research Collaborative Access Team, 1994-  
Assoc. Chair, Dept. of Biological, Chemical and Physical Sciences, 1993-1999  
Staff Associate, Intl. Centre for Science and High Technology, Trieste, Italy, 1990-1993  
Visiting Senior Scientist, Intl. Centre for Theoretical Physics, Trieste, Italy, 1989-1990  
Associate Professor of Physics, IIT, 1989-  
Assistant Professor of Physics, IIT, 1983-1989  
NATO Research Fellowship (declined)  
Postdoctoral Research Fellow, Department of Physics, Rutgers University, 1981-1983

#### Research Expertise

Over the past 12 years my research has focussed on structural studies of complex oxide materials through x-ray and neutron diffraction and spectroscopy. Materials studied include high temperature superconductors and oxygen-permeable membrane materials. In the past five years, I have dedicated most of my time to the construction and commissioning of the Materials Research Collaborative Access Team (MRCAT) beamlines at the Advanced Photon Source, where I have served as the Associate Director and the overall project manager.

#### Selected Publications (chronological order)

- “Oxygen Ordering and Superconductivity in  $\text{La}(\text{Ba}_{2-x})\text{La}_x\text{Cu}_3\text{O}_{7+\delta}$ ”, C.U. Segre, B. Dabrowski, D.G. Hinks, K. Zhang, J.D. Jorgensen, M.A. Beno and I.K. Schuller, *Nature* **329**, 227 (1987).
- “Structural Behavior and Chemical Order of Fe in  $\text{YBa}_2(\text{Cu}_{1-x}\text{Fe}_x)_3\text{O}_{7+\delta}$ ”, B.D. Dunlap, J.D. Jorgensen, C.U. Segre, A.E. Dwight, J.L. Matykiewicz, H. Lee, W. Peng and C.W. Kimball, *Physica C* **158**, 397 (1990).
- “Structure and Superconductivity in the Single Cu-O Layered  $(\text{Bi}_{2-x}\text{Pb}_x)(\text{Sr}_{2-y}\text{La}_y)\text{CuO}_{6+\delta}$  System”, K. Zhang, B.H. Ma and C.U. Segre, *Physica C* **179**, 405 (1991).
- “Superconductivity and Charge Transfer Compensation by Direct Doping in the  $\text{La}_{1+x}\text{Ca}_y\text{Ba}_{2-x-y}\text{Cu}_3\text{O}_{7+\delta}$  System”, T. Mertelj, P. Stastny, F.C. Matacotta, P. Ganguly, C.U. Segre and D. Mihailovic, *Physica C* **179**, (1991).
- “Structural Inhomogeneities in Oxygen-Deficient  $\text{ErBa}_2\text{Cu}_3\text{O}_{6+\delta}$  Associated with the Tetragonal-to-Orthorhombic Transition: Evidence of First Order Behavior”, P.G. Radaelli, C.U. Segre, D.G. Hinks and J.D. Jorgensen, *Phys. Rev.*, **B45**, 4923 (1992).
- “Transport Properties and Defect Structure of  $\text{SrFeCo}_{0.5}\text{O}_x$ ”, B. Ma, U. Balachandran, J-H. Park and C.U. Segre, *J. Electrochem. Soc.* **143**, 1736 (1996).
- “Humidity Sensing Properties of Nafion and Sol-Gel Derived  $\text{SiO}_2/\text{Nafion}$  Composite Thin Films”, C.D. Feng, S.L. Sun, H. Wang, C.U. Segre and J.R. Stetter, *Sensors & Actuators B-Chemical* **40**, 217-222 (1997).
- “Methanol Oxidation in Single-Phase Pt-Ru-Os Ternary Alloys”, K.L. Ley, R.X. Liu, C. Pu, Q.B. Fan, N. Leyarowska, C.U. Segre and E.S. Smotkin, *J. Electrochem. Soc.* **144**, 1543-1548 (1997).



## Bruce A. Bunker, Co-PI

Physics Department  
University of Notre Dame  
333G Nieuwland Science, Notre Dame, IN 46556  
Voice: (219) 631-7219; Fax: (219) 631-5952  
e-mail: Bruce.Bunker.1@nd.edu

Ph.D. University of Washington, 1980

### Post Ph.D. Activities and Honors

Director, Materials Research Collaborative Access Team  
Member, Research Directorate, Advanced Photon Source  
Member, Executive Committee of the International XAFS Society  
Member, X11A and X23A2 Participating Research Team, National Synchrotron Light Source  
Member, National Synchrotron Light Source Proposal Study Panel, 1993-1998  
Member, National Science Foundation Materials Science Proposal Review Panel, May, 1993  
Department Chair, University of Notre Dame. August 1998 - present.  
Professor of Physics, University of Notre Dame. August 1994 - present.  
Associate Professor of Physics, University of Notre Dame. 1987-1994.  
Assistant Professor of Physics, University of Notre Dame. 1983-1987  
IBM Postdoctoral Fellow, University of Illinois, Urbana-Champaign, 1981-1983  
Postdoctoral Research Associate, Materials Research PRT, Brookhaven National Laboratory, 1981  
Postdoctoral Research Associate, University of Washington, 1980

### Selected Publications

- "XAFS Studies of Fe Sites in Synthetic and Natural Neuromelanins," J. Kropf, B.A. Bunker, M. Eisner, S.C. Moss, L. Zecca, A. Stroppolo, and P.R. Crippa, *Biophys J.* **75**, 3135-3142 (1998).
- "X-ray Study of Atomic Correlations in ZnCdSeTe Epitaxial Thin Films," Q. Lu, B. A. Bunker, H. Luo, A. J. Kropf, K. M. Kemner, J. K. Furdyna, *Phys. Rev.* **B55**, 9910 (1997).
- "Observation of anisotropic vibrational amplitudes due to thermal motion at the Cu/Al<sub>2</sub>O<sub>3</sub> interface," R.M. Mayanovic and B.A. Bunker, *Phys. Lett. A* **202**, 225-229 (1995).
- "Atomic rearrangement at interfaces in ZnTe/CdSe superlattices," K.M. Kemner, B.A. Bunker, H. Luo, N. Samarth, J.K. Furdyna, M.R. Weidmann, K.E. Newman, *Phys. Rev.* **B50**, 4327 (1994).
- "X-ray Studies of Off-Center Ions and Ferroelectricity in PbS<sub>x</sub>Te<sub>1-x</sub> and Zn<sub>x</sub>Cd<sub>1-x</sub>Te Alloys," B.A. Bunker, Z. Wang, Q. Islam, *Ferroelectrics* **150**, 171 (1993).
- "EXAFS Studies of the Ferroelectric Phase Transitions Induced By Off-center Ions in PbS<sub>x</sub>Te<sub>1-x</sub> and Zn<sub>x</sub>Cd<sub>1-x</sub>Te Alloys," Z. Wang, B.A. Bunker, R.A. Mayanovic, U. Debska, J.K. Furdyna and Q.T. Islam, invited review paper, *Modern Phys. Lett.* **6**, 1413 (1992).
- "X-ray absorption fine-structure studies of PbS<sub>x</sub>Te<sub>1-x</sub> alloys: ferroelectric phase transitions induced by off-center ions," Z. Wang and B.A. Bunker, *Phys. Rev.* **B46**, 11277 (1992).
- "XAFS Investigations of Ferroelectric Semiconductors," B.A. Bunker, Z. Wang, Quazi Islam, *Ferroelectrics* **120**, 23 (1991).
- "Studies of atomic correlations in quaternary semiconductor alloys using the Extended X-ray Absorption Fine Structure technique", S. I. Islam and B. A. Bunker, *Phys. Lett.* **156**, 247 (1991).
- "XAFS and X-ray Reflectivity Studies of Buried Interfaces," B.A. Bunker, A.J. Kropf, K.M. Kemner, R.A. Mayanovic, and Q. Lu, *Nuc. Inst. Meth. Phys. Res. B* **133**, 102 (1997).



## Randolph S. Duran, Co-PI

Department of Chemistry  
University of Florida  
P.O. Box 117200, Gainesville, FL 32611  
Voice: (352) 392-2011  
e-mail: duran@chem.ufl.edu

Ph.D. , University Louis Pasteur, Charles Sadron Institute, France. 1987

### Post Ph.D. Activities and Honors

Lavoisier Scholarship, Scientific Mission of the French Embassy, 1986-88  
Post Doctoral Scholarship, Max Planck Institute, Mainz, Germany, Aug. 1987 to July 1988  
Post Doctoral Scholarship, National Institute for Standards and Technology, July 1988 to July 1989  
Assistant Professor, Dept. of Chemistry, Univ. of Florida, Gainesville, FL, 1989-1994  
Research Achievement Award, University of Florida, 1991  
National Science Foundation Young Investigator Award, 1993-98  
NRL Alan Berman Research Publication Award, 1994  
Editorial Board, Supramolecular Science  
Executive Committee Member, APS MRCAT Beamline, 1996-present  
Associate Professor, Dept. of Chemistry, Univ. of Florida, Gainesville, FL, 1994-

### Selected Publications

- "Blends of a Ferroelectric Copolymer with Monomer at the Air/Water Interface", A. F. Thibodeaux, U. Radler, J. Naciri, J. Ruth, R. Shashidhar, R.S. Duran, *Macromolecules*, **27**, 784 (1994).
- "X-ray Investigations of Langmuir-Blodgett Multilayer Films of a Side Chain Liquid Crystalline Copolymer", R. Geer, S. Qadri, R. Shashidhar, A. Thibodeaux, and R. S. Duran, *Liq. Crystals*, **16**, 869 (1994).
- "Magnetic Field Orientation of Liquid Crystalline Epoxy Thermosets", B.C. Benicewicz, M.E. Smith, J.D. Earls, R.D. Priester, Jr., S.M. Setz, R.S. Duran, and E. P. Douglas, *Macromolecules*, **31**, 4730-473 (1998).
- "Two- and Three-Dimensional Nanoparticles of Liquid Crystals Prepared at the Air/Liquid Interface", T.E. Herod and R.S. Duran, *Langmuir*, **14**, 6606 (1998).
- "Off-specual X-ray Scattering in Langmuir-Blodgett Multilayers of a Liquid-Crystallization Polymer", R.E. Geer, S.B. Qadri, R. Shashidhar, A.F. Thibodeaux and R.S. Duran, *Physical Review* **E52**, 671 (1995).
- "Measurement of Line Tension from Cell Coalescence Events in a Langmuir Film", M.J. Roberts, E.J. Teer and R.S. Duran, *J. Phys. Chem.*, **101**, 699 (1997).
- "Synthesis and Characterization of C60 End-Capped Poly(ethyleneoxyde) Stars", D. Taton, S. Angot, Y. Gnanou, E. Wolert, and R. Duran, *Macromolecules*, **31**, 6030 (1998).
- "Polymer Dispersed Liquid Crystal Monolayers", T.E. Herod and R.S. Duran, *Langmuir*, **24**, 6956 (1998).







## **Pulak Dutta, Co-PI**

Department of Physics and Astronomy  
Northwestern University  
2145 Sheridan Road, Evanston, IL 60208  
Voice: (847) 491-5465; Fax: (847) 491-9982  
e-mail: pdutta@nwu.edu

Ph.D. University of Chicago, 1980

### **Post Ph.D. Activities and Honors**

Fellow, American Physical Society 1993-

Professor, Northwestern University, Dept. of Physics & Astronomy 1992-

Associate Professor, Northwestern University, Dept. of Physics & Astronomy 1987-92

Assistant Professor, Northwestern University, Dept. of Physics & Astronomy 1981-1987

Argonne National Laboratory, Postdoctoral Appointee, 1981-1983

### **Selected Publications**

- "Structure and phase transitions in Langmuir monolayers", V.M. Kaganer, H. Möhwald and P. Dutta, *Revs. Mod. Phys.* **71**, 779 (1999).
- "Observation of molecular layering in thin liquid films using X-ray reflectivity", C.-J. Yu, A. G. Richter, A. Datta, M. K. Durbin and P. Dutta, *Phys. Rev. Lett.*, **82**, 2326 (1999).
- "Backbone orientational order in fatty acid monolayers at the air-water interface", M.K. Durbin, A. Richter, C.-J. Yu, J. Kmetko, J.M. Bai and P. Dutta, *Phys. Rev.* **E58**, 7686 (1998).
- "An *in-situ* X-ray reflectivity study of the deposition of self-assembled monolayers from solution", A.G. Richter, M.K. Durbin, C.J. Yu and P. Dutta, *Langmuir* **14**, 5980 (1998).
- "Ordered phases in Langmuir monolayers of an azobenzene derivative", M.K. Durbin, A. Malik, A.G. Richter, C.-J. Yu, P. Dutta, *Langmuir* **14**, 899 (1998).
- "Molecular Self-Assembly Routes To Electroluminescent Multilayer Structures", Weijin Li, Joshua E. Malinsky, Homer Chou, Wuping Ma, Lifeng Geng, Tobin J. Marks, Ghassan E. Jabbour, Sean E. Shaheen, Bernard Kippelen, Nasser Peyghambarian, Pulak Dutta, Andrew G. Richter, Neal R. Armstrong, Paul A. Lee, and Jeffrey D. Anderson, *Polymer* **39**, 1083 (1998).
- "Specular X-ray reflectivity studies of microstructure and ordering in self-assembled multilayers", A. Malik, W. Lin, M.K. Durbin, T.J. Marks, and P. Dutta, *J. Chem. Phys.* **107**, 645 (1997).
- "Transitions to a new chiral phase in a Langmuir monolayer", M.K. Durbin, A. Malik, A.G. Richter, R. Ghaskadvi, T. Gog and P. Dutta, *J. Chem. Phys.* **106**, 8216 (1997).
- "In Situ X-ray diffraction study of Langmuir-Blodgett deposition", M.K. Durbin, A. Malik, A.G. Richter, K.G. Huang and P. Dutta. *Langmuir*, **13**, 6547 (1997).
- "Studies of monolayers using synchrotron X-ray diffraction", P. Dutta, *Curr. Opinion Solid St. Mat. Sci.* **2**, 557 (1997).



## 7 References

### References

- [1] T. Shibata, B. A. Bunker, Z. Zhang, D. Meisel, C. F. Vardeman, and J. D. Gezelter, *J. Am. Chem. Soc.* **124**, 11989 (2002), and references therein.
- [2] D.S. Cameron, G.A. Hards, and D. Thomsett, *Proc. Workshop on Direct Methanol-Air fuel cells*, A.R. Landgrebe, R.K. Sen, and D.J. Wheeler, ed. **PV92-14**, pp. 10-23 (The Electrochemical Society, Proceeding Series, Pennington, NJ 1992).
- [3] Watanabe M., Uchida, M, Motoo, S, *J. Electroanal. Chem.* **229**, 395 (1987).
- [4] W.E. O'Grady, P.L. Hagans, K.I. Pandya, D.L. Maricle; *Langmuir* **17**, 3047-3050 (2001).
- [5] James McBreen and Sanjeev Mukerjee, *J. Electrochem. Soc.*, **142**, 3399-3404 (1995).
- [6] Sanjeev Mukerjee and James McBreen, *J. Electroanal. Chem.* **448**, 163-171 (1998).
- [7] T. Page, R. Johnson, J. Hormes, S. Noding, B. Rambabu, *J. Electroanal. Chem.* **485**, 34-41 (2000).
- [8] Andrea E. Russel, Stephanie Maniguet, Rebecca Mathew, Jun Yao, Mark A. Roberts, David Thompsett *Journal of Power Sources* **96**, 226-232 (2001).
- [9] Gurau B., Viswanathan R., Liu R., Lafrenz T. J, Ley K. L, Smotkin E. S., Reddington E., Sapienza A., Chan B., Mallouk T.E., Sarangapani S., *J.Phys.Chem B* **102**, 9997-10003 (1998).
- [10] R. Viswanathan, G. Hou, R. Liu, S.R. Bare, F. Modica, G. Mickelson, C.U. Segre, N.E. Leyarowska, T. Chikyow and E.S. Smotkin, *J. Phys. Chem. B* **106**, 3458 (2002).
- [11] R. Viswanathan, R. Liu and E.S. Smotkin, *Rev. Sci. Inst.* **75**, 2124 (2002).
- [12] N. Dimakis, G. Bunker, H. Iddir and E.S. Smotkin, private communication.
- [13] G. Blyholder, *J. Phys. Chem.* **68**, 2772 (1964).
- [14] M.S. Wilson, S. Gottesfeld, *J. Appl. Electrochem.* **22**, 1 (1992).
- [15] M.E. Herron, S.E. Doyle, S. Pizzini, K.J. Roberts, J. Robinson, G. Hards, F.C. Walsh, *J. Electroanal. Chem.* **324**, 243 (1992).
- [16] S. Maniguet, R. J. Mathew, A. Russel, *J.Phys.Chem B* **104**,1998-2004 (2000).
- [17] A. Kolics and A. Wieckowski, *J. Phys. Chem. B* **105**, 2588-2595 (2001).
- [18] B.C. Schardt, J.L. Stickney, D.A. Stern, A. Wieckowsk,D.C. Zapien, A.T. Hubbard, *Surf. Sci.* **175**, 520 (1986).
- [19] Zelenay P., Wieckowski A. In *Electrochemical Interfaces: Modern Techniques for In-situ surface characterization*; H. Abruna, Ed. p479 (VCH Publishers: New York, 1991).; p 479
- [20] S. Mukerjee, S. Srinivasan, M. Soriaga, J. McBreen, *J.Phys.Chem.* **99**, 4577 (1995).
- [21] A.L. Ankudinov, B. Ravel, J.J. Rehr, and S.D. Conradson, *Phys. Rev. B* **58**, 7565 (1998).
- [22] H.A. Gasteiger, N. Markovic, P.N. Ross, and E.J. Cairns, *J. Electrochem. Soc.* **141**, 1795-1803 (1994).

- [23] R. Liu, H. Iddir, Q. Fan, G. Hou, A. Bo, K. L. Ley, E. S. Smotkin, Y. E. Sung, H. Kim, S. Thomas, A. Wieckowski *J. Phys. Chem. B*, **104**, 3518-3531 (2000).
- [24] W. F. Lin, T. Iwasita, W.J. Vielstich, *J. Phys. Chem. B* **103**, 3250 (1999).
- [25] Deryn Chu and Sol Gilman, *J. Electrochem. Soc.* **143**, 1685-1690 (1996).
- [26] J.W. Long, R.M. Stroud, K.E. Swider-Lyons, D. R. Rolison, *J Phys. Chem. B* **104**, 9772-9776 (2000).
- [27] see e.g. V.M. Kaganer, H. Möhwald and P. Dutta, *Revs. Mod. Phys.* **71**, 779 (1999) .
- [28] e.g. S. Mann, in *Inorganic Materials*; D.W. Bruce, D. O'Hare, Eds. (Wiley: Chichester, England, 1992).
- [29] J. Kmetko, A. Datta, G. Evmenenko, M.K. Durbin, A.G. Richter, P. Dutta, *Langmuir* **17**, 4697 (2001).
- [30] M.I. Boyanov, J. Kmetko, T. Shibata, A. Datta, B.A. Bunker, and P. Dutta, submitted to *Phys. Rev. B*.
- [31] e.g. Mann, S. *Biomaterialization: Principles and Concepts in Bioinorganic Materials Chemistry*, (Oxford UP: New York, 2001).
- [32] Jan Kmetko, Chungjong Yu, Guennadi Evmenenko, Sumit Kewalramani, Pulak Dutta, *Phys. Rev. Lett.* **89**, 186102 (2002).
- [33] M.I. Boyanov, S.D. Kelly, K.M. Kemner, B.A. Bunker, J.B. Fein, D.A. Fowle, to be published in *Geochimica et Cosmochimica Acta*.
- [34] <http://www.em.doe.gov/emprimer/appb.html>.
- [35] L.E. MaCaskie, and G. Basnakova, *Environmental Science & Technology* **32**, 184 (1998).
- [36] S. Baron, *Medical Microbiology*, 4<sup>th</sup> ed. University of Texas Medical Branch, (1996).
- [37] D.R. Lovley, *Annual Review of Microbiology* **47**, 263 (1993).
- [38] T. Schiott, T, "Cytochrome c biogenesis in *Bacillus subtilis*. Identification and analysis of ccdA", Dissertation, Lund University (1999).
- [39] J.R. Postgate, *The sulfate-reducing bacteria*, 2<sup>nd</sup> ed. Cambridge University Press, (1984).
- [40] D.R. Lovley and E.J.P. Phillips, *Environmental Science and Technology* **26**, 2228 (1992).
- [41] C.-J. Yu, A. G. Richter, J. Kmetko, A. Datta and P. Dutta, *Europhys. Lett.* **50**, 487 (2000).
- [42] C.-J. Yu, A. G. Richter, A. Datta, M. K. Durbin and P. Dutta, *Phys. Rev. Lett.* **82**, 2326 (1999).
- [43] H. Reichert, O. Klein, H. Dosch, V. Henkimald, T. Lippmann and G. Reiter, *Nature* **408**, 839 (2000).
- [44] e.g. J. van Alsten and S. Granick, *Phys. Rev. Lett.* **61**, 2570 (1988).
- [45] J.N. Israelachvili and S.J. Kott, *J. Coll. Interf. Sci.* **129**, 461 (1989).
- [46] M.A. Smith, P.L.R. Harris, L.M. Sayre, G. Perry, *Proc. Natl. Acad. Sci. USA* **94**, 9866-9868 (1997).
- [47] M.A. Lovell, J.D. Robertson, W.J. Teesdale, J.L. Campbell, W.R. Markesbery, *J. Neurol. Sci.* **158**, 470-52 (1998).

- [48] Beard, J.L., J.R. Connor, B.C. Jones, *Nutr. Rev.* **51**, 157-170 (1993).
- [49] P. Fisher, M.E. Gotz, W. Danielczyk, W. Gsell, P. Riederer, *Life Sci.* **60**, 2273-2278 (1997).
- [50] P.P. Perl and P.F. Good, *Ann. Neurol.* **32**, S76-S81 (1992).
- [51] L. Goodman, *J. Nerv. Ment. Dis.* **118**, 97-130 (1953).
- [52] L.M. Sayre, G. Perry, P.L.R. Harris, Y.H. Liu, K.A. Schubert, M.A. Smith, *J. Neurochem* **74**, 270-279 (2000).
- [53] J. Dobson, *FEBS Lett.* **496**, 1-5 (2001).
- [54] J.R. Connor, K.L. Boeshore, S.A. Benkovic, *Mol. Biol. Cell.* **3**, 84A (1992).
- [55] D.A. Loeffler, J.R. Connor, P.L. Juneau, B.S. Snyder, L. Kanaley, A.J. Demaggio, H. Nguyen, C.M. Brickman, P.A. Lewitt, *J. Neurochem.* **65**, 710-716 (1995).
- [56] A.R.J. Curtis, and 15 others, *Nature Genetics* **28**, 350-354 (2001).
- [57] B. Zhou, S.K. Westway, B. Levinson, M.A. Johnson, J. Gitschier, S.J. Hayflick, *Nature Genetics* **28**, 345-349 (2001).
- [58] J. Dobson, *Cell. Mol. Biol.* **OL47**, 49-50 (2001).
- [59] J.L. Kirschvink, A. Kobayashi-Kirschvink, B.J. Woodford, *Proc. Natl. Acad. Sci., USA* **89**, 7683-7687 (1992).
- [60] R.P. Blakemore, *Science* **190**, 377-379 (1975).
- [61] B.A. Bazylnski, B.R. Heywood, S. Mann & R. Frankel, *Nature* **366**, 218 (1993).
- [62] J.L. Kirschvink, D.S. Jones, *Magnetite biomineralization and magnetoreception in organisms: A new biomagnetism*, B.J. MacFadden, Eds., (R.P. Plenum Publishing Corp. New York, 1985).
- [63] J.R. Dunn, M. Fuller, J. Zoeger, J. Dobson, F. Heller, E. Caine and B.M. Moskowitz, *Brain Res. Bull.* **36**, 149-153 (1995).
- [64] J. Dobson, and P. Grassi, *Brain Res. Bull.* **39**, 255-259 (1996).
- [65] P.P. Schultheiss-Grassi and J. Dobson, *BioMetals.* **12**, 67-72 (1999).
- [66] C. Qunitana, M. Lancin, C. Marhic, M. Pérez, , J. Avila, J.L. Carrascosa, *Cell. & Molec. Biol.* **46**, 807-820 (2000).
- [67] J.C. Scaiano, S. Monahan, J. Renaud, *Photochem. Photobiol.* **65**, 759-762 (1997).
- [68] F.Q. Schafer, S.Y. Qian, G.R. Buettner, *Cell. Molec. Biol.* **46**, 657-662 (2000).
- [69] J. Dobson, *Exper. Brain Res.* In Press.
- [70] J. Dobson, T.G. St. Pierre, H. Pardoe, P.P. Schultheiss-Grassi, *Electricity and Magnetism in Biology and Medicine*, ed. S. Bersani. Plenum, New York, 401-404 (1999).
- [71] J.A. Edwardson, J. Klinowski, A.E. Oakley, R.H. Perry, J.M. Candy, *Ciba Found. Symp.* **121**, 160-172 (1986).

- [72] S.E. Asher, F.S. Hasoon, R.A. Gessert, M.R. Young, P. Sheldon, J. Hiltner, and J. Sites, *28th IEEE PVSC-2000*.
- [73] D. Grecu and A.D. Compaan, *Appl. Phys. Lett.* **75**, 361-363 (1999).
- [74] J. F. Ziegler, *The Stopping and Range of Ions in Matter*, Volumes **2 - 6**, Pergamon Press, 1977-1985.
- [75] J. P. Biersack and L. Haggmark, *Nucl. Instr. and Meth.*, **174**, 257, (1980) (program available at <http://www.srim.org/>).
- [76] D. Mao, L. H. Feng, Y. Zhu, J. Tang, W. Song, R. Collins, D. L. Williamson, and J. U. Trefny in *13th NREL Photovoltaics Program Review Proc.*, AIP Conference Proc. **353**, 352 (1996).
- [77] B. E. McCandless, I Youm and R. W. Birkmire, *Prog. Photovolt. Res. Appl.* **7**, 21 (1999).
- [78] [B1] <http://www.med.sc.edu/RADIOLO/4nucmed.htm>.
- [79] [B2]
- [80] [B3] <http://www.fda.gov/cder/guidance/old030fn.pdf>.
- [81] [B4]
- [82] [B5]
- [83] [Z1]
- [84] [Z2]
- [85] [Z3]
- [86] [Z4]
- [87] M.R. Pederson and S.N. Khanna, *Phys. Rev. B* **60**, 9566 (1999).
- [88] T. Lis, *Acta Cryst. B* **36**, 2042 (1980).
- [89] R. Sessoli, H.L. Tai, A.R. Schake, S. Wang, J.B. Vincent, K. Folting, D. Gatteschi, G. Christou and D.N. Hendrickson, *J. Am. Chem. Soc.* **115**, 1804 (1993).
- [90] G. Christou, D. Gatteschi, D.H. Hendrickson, and R. Sessoli, *MRS Bulletin* **25**, 66 (2000).
- [91] M. Clemente-Leon, H. Soyer, E. Coronado, C. Mingotaud, C.J. Gomez-Garcia, and P. Delhaes, *Angew. Chem. Inter.* **37**, 2842 (1998).
- [92] N.E. Leyarovska, M. Soler, G. Christou, and J. Terry, in preparation.
- [93] C.-D. Park, and D.-Y. Jung, *Bull. Kor. Chem. Soc.* **22**, 611 (2001).
- [94] A.L. Ankudinov, personal communication.
- [95] H. Kung, *Transition Metal Oxides: Surface Chemistry and Catalysis*, (Elsevier: New York, 1989); I.M. Campbell, *Catalysis at Surfaces*, (Chapman and Hall, London, 1988); J.M. Thomas, *Angew. Chem. Int. Ed. Engl.* **33**, 913 (1994); J.M. Thomas, W.J. Thomas, *Principles and Practice of Heterogeneous Catalysis*, (VCH, Weinheim, 1997); J.M. Thomas, R. Raja, G. Sankar, R.G. Bell, *Nature*, **398**, 227 (1999).

- [96] Z.R. Ismagilov, M.A. Kerzhentsev, T.L. Susharina, *Russ. Chem. Rev.* **59**, 973 (1990); M. Shelef, *Chem. Rev.* **95**, 209 (1995).
- [97] G. Centi, F. Trifiro, J.R. Ebner, V.R. Franchetti, *Chem. Rev.* 1988, **88**, 55 (1988).
- [98] R.K. Grasselli, J.D. Burrington, *Adv. Catal.*, **30**, 133 (1981).
- [99] B.C. Gates, *Catalytic Chemistry*, (Wiley: New York, 1992) Chapter 6.
- [100] M.T. Pope, *Heteropoly and Isopoly Oxometalates* (Springer: Berlin, 1983).
- [101] M.T. Pope, A. Müller, *Angew. Chem. Int. Ed. Engl.* **30**, 34 (1991).
- [102] *Polyoxometalates: From Platonic Solids To Anti-Retroviral Activity*, M.T. Pope, A. Müller, Eds., (Kluwer Academic: Dordrecht, 1994).
- [103] See the following special issue dedicated to this field: *Chem. Rev.* **98**, 1-390 (1998).
- [104] See, D.E. Katsoulis, *Chem. Rev.* **98**, 359 (1998), and references therein.
- [105] W.P. Griffith, *Trans. Met. Chem.* **16**, 548 (1991).
- [106] N. Mizuno, M. Misono, *Chem. Rev.* **98**, 199 (1998).
- [107] Y. Izumi, K. Urabe, M. Onaka, *Zeolite, Clay, and Heteropoly Acid in Organic Reactions*, (VCH, Weinheim, 1992).
- [108] M. Pohl, D.K. Lyon, N. Mizuno, K. Nomiya, R.G. Finke, *Inorg. Chem.* **34**, 1413 (1995) and references therein.
- [109] (a) Müller, A.; Koegerler, P.; Kuhlmann, C. A Variety of Combinatorially Linkable Units as Disposition: From A Giant Icosahedral Keplerate to Multi-Functional Metal-Oxide Based Network Structures. *Chem. Commun.* 1999, 1347-1358. (b) Khan, M. I.; Chen, Q.; Salta, J.; O'Connor, C. J.; Zubietta, J. Retention of Structural Cores in the Synthesis of High Nuclearity Polyoxomolybdate Clusters Encapsulating {Na(H<sub>2</sub>O)<sub>3</sub>} and {MoO<sub>3</sub>} Moieties. *Inorg. Chem.*, 1996, 35, 1880-1901. (c) Müller, A.; Sarkar, S.; Shah, S. Q. N.; Boegge, H.; Schmidtmann, M.; Sarkar, Sh.; Koegerler, P.; Hauptfleisch, B.; Trautwein, A.; Schuenemann, V. Archimedean Synthesis and Magic Numbers: Sizing Giant Molybdenum Oxide Based Molecular Spheres of the Keplerate Type. *Angew. Chem. Int. Ed. Engl.*, 1999, 38, 3238-3241. (d) Müller, A.; Peters, F.; Pope, M. T.; Gatteschi, D. Polyoxometalates: Very Large Clusters - Nanoscale Magnets. *Chem. Rev.* 1998, 98, 239.
- [110] W.G. Klemperer, T.A. Marquart, O.M. Yaghi, *Angew. Chem. Int. Ed. Engl.* **31**, 49 (1992).
- [111] W.G. Klemperer, C.G. Wall, *Chem. Rev.* **98**, 297 (1998).
- [112] K. Isobe, A. Yagasaki, *Acc. Chem. Res.* **26**, 524 (1993).
- [113] M.I. Khan, E. Yohannes, D. Powell, *J. Chem. Soc., Chem. Comm.*, **23** (1999).
- [114] M.I. Khan, E. Yohannes, D. Powell, *Inorg. Chem.* **38**, 212 (1999).
- [115] M.I. Khan, E. Yohannes, R.J. Doedens, *Angew. Chem. Int. Ed. Engl.* **38**, 1292 (1999).
- [116] J.T. Miller, C.L. Marshall, A.J. Kropf, *J. Catalysis* **202**, 89-99 (2001).

- [117] A.J. Kropf, H. Tostmann, C.S. Johnson, J.T. Vaughey, M.M. Thackeray, *Electrochem. Commun.* **3**, 244-251 (2001).
- [118] T. Lis, *Acta Crystallographica* **B36**, 2042 (1980).
- [119] R. Sessoli R., H.L. Tai, A.R. Schake, S. Wang, J.B. Vincent, K. Folting, D. Gatteschi, G. Christou, and D.N. Hendrickson, *J. Am. Chem. Soc.* **115**, 1804 (1993).
- [120] V. Petkov, S. Billinge, T.Vogt, A. Ichimura, J. Dye, *Phys. Rev. Lett.* **89**, 075502 (2002).
- [121] J. Manriquez, G. Yee, R. McLean, A. Epstein, J. Miller, *Science* **252**, 1415 (1991).
- [122] S. Castro, Z. Sun, C. Grant, J. Bollinger, D. Hendrickson, G. Christou, *J. Am. Chem. Soc.* **120**, 2365 (1998).
- [123] K.R. Finnie, R. Haasch, R.G. Nuzzo, *Langmuir* **16**, 6968 (2000).
- [124] J.W. Zheng, Z.H. Zhu, H.F. Chen, Z.F. Liu, *Langmuir* **16**, 4409 (2000).
- [125] W. Tsukruk, *Adv. Mater.* **13**, 95 (2001).
- [126] G.K. Jennings, J.C. Munro, T.H. Yong, P.E. Laibinis, *Langmuir* **14**, 6130 (1998).
- [127] A. Ulman, *Chem. Rev.* **96**, 1533 (1996).
- [128] A.G. Richter, M.K. Durbin, C.-J. Yu, L. Dutta, *Langmuir* **14**, 5980 (1998).
- [129] S.R. Cohen, R. Naaman, J. Sagiv, *J. J. Phys. Chem.* **90**, 3054 (1986).
- [130] D.K. Schwartz, S. Steinberg, J. Israelachvili, J.A.N. Zasadzinski, *Phys. Rev. Lett.* **69**, 3354 (1992).
- [131] K. Bierbaum, M. Grunze, A.A. Baski, L.F. Chi, W. Schrepp, H. Fuchs, *Langmuir* **11**, 2143 (1995).
- [132] J. Sagiv, *J. Am. Chem. Soc.* **102**, 92 (1980).
- [133] P. Silberzan, L. Leger, D. Ausserre, J. Benattar, *J. Langmuir* **7**, 1647 (1991).
- [134] R. Resch, M. Grasserbauer, G. Friedbacher, T. Vallant, H. Brunner, U. Mayer, H. Hoffmann, *Appl. Surf. Sci.* **140**, 168 (1999).
- [135] S.R. Wasserman, G.M. Whitesides, I.M. Tidswell, B.M. Ocko, P.S. Pershan, J.D. Axe, *J. Am. Chem. Soc.* **111**, 5852 (1989).
- [136] T. Vallant, J. Kattner, H. Brunner, U. Mayer, H. Hoffmann, *Langmuir* **15**, 5339 (1999).
- [137] A. Ulman, *An Introduction to Ultrathin Organic Films : From Langmuir-Blodgett to Self-Assembly*, (Academic Press: Boston, 1991).
- [138] P. Dutta, J.B. Peng, B. Lin, J.B. Ketterson, M. Prakash, P. Georgopoulos, S. Ehrlich, *Phys. Rev. Lett.* **58**, 2228 (1987).
- [139] K. Kjaer, J. Als-Nielsen, C.A. Helm, L.A. Laxhuber, H. Mohwald, *Phys. Rev. Lett.* **58**, 2224 (1987).
- [140] S. Vidon, R.M. Leblanc, *J. Phys. Chem. B* 1998, **102**, 1279 (1998).
- [141] D.W. Britt, V.J. Hlady, *Phys. Chem. B* **103**, 2749 (1999).

- [142] S.R. Carino, R.S. Duran, R.H. Baney, L.A. Gower, L. He, P.K. Sheth, *J. Am. Chem. Soc.* **123**, 2103 (2001).
- [143] J. Sjöblom, G. Stakkestad, H. Ebeltoft, S.E. Friberg, P. Claesson, *Langmuir* **11**, 2652 (1995).
- [144] J.-L. Brosseau, S. Vidon, R.M. Leblanc, *J. Chem. Phys.* **108**, 7391 (1998).
- [145] S.R. Carino, H. Tostmann, R.S. Underhill, J. Logan, G. Weerasekera, J. Culp, M. Davidson, R.S. Duran, *J. Am. Chem. Soc.* **123**, 767 (2001).
- [146] W. M. Lavender, *Synchrotron Radiation Instrumentation: Eleventh US National Conference*, AIP Conf. Proc. **521**, 332 (2000).